



Deposited via The University of Leeds.

White Rose Research Online URL for this paper:

<https://eprints.whiterose.ac.uk/id/eprint/168379/>

Version: Accepted Version

Article:

Komissarov, SS (Cover date: September 2023) Balanced carving turns in alpine skiing. Sports Biomechanics, 22 (9). pp. 1209-1242. ISSN: 1476-3141

<https://doi.org/10.1080/14763141.2020.1795236>

© 2020 Informa UK Limited, trading as Taylor & Francis Group. This is an author produced version of an article published in Sports Biomechanics. Uploaded in accordance with the publisher's self-archiving policy.

Reuse

Items deposited in White Rose Research Online are protected by copyright, with all rights reserved unless indicated otherwise. They may be downloaded and/or printed for private study, or other acts as permitted by national copyright laws. The publisher or other rights holders may allow further reproduction and re-use of the full text version. This is indicated by the licence information on the White Rose Research Online record for the item.

Takedown

If you consider content in White Rose Research Online to be in breach of UK law, please notify us by emailing eprints@whiterose.ac.uk including the URL of the record and the reason for the withdrawal request.

Balanced pure carving turns in alpine skiing

Serguei S. Komissarov
Department of Applied Mathematics
The University of Leeds
Leeds, LS2 9JT, UK

Abstract

In this paper we analyse the model of pure carving turns in alpine skiing and snowboarding based on the usual assumption of approximate balance between forces and torques acting on the skier during the turn. The approximation of torque balance yields both lower and upper limits on the skier speed, which depend only on the sidecut radius of skis and the slope gradient. We use the model to simulate carving runs on slopes of constant gradient and find that pure carving is possible only on slopes of relatively small gradient, with the critical slope angle in the range of $8^\circ - 20^\circ$. The exact value depends mostly on the coefficient of snow friction and to a lesser degree on the sidecut radius of skis. Comparison with the practice of ski racing shows that the upper speed limit and the related upper limit on the slope gradient set by the model are too restrictive and so must be the assumption of torque balance used in the model. A more advanced theory is needed.

Keywords: alpine skiing, modelling, balance/stability, performance

Introduction

When making their way down the hill, expert skiers execute complex coordinated body movements, often within a fraction of a second, which allow them to ski at speed and yet to remain in control. Their decisions are dictated by many factors, such as terrain, snow condition, equipment, etc. A ski racer faces additional challenges as a race course significantly reduces the freedom of choosing trajectory. There is a great deal of qualitative understanding of skiing techniques and race tactics based on the personal experiences of ski professionals, coaches and instructors (e.g. LeMaster, 2010). However, this empirical knowledge is imprecise, very subjective and sometimes even subconscious, and this keeps the door open to misunderstanding, misconceptions and controversies.

19 Scientific approach can help to put the understanding of skiing on a more solid
20 footing by using the well-tested basic principles of mechanics (including biomechan-
21 ics) and exploring various aspects of physical interactions specific to skiing. In fact,
22 there has already been a great deal of research in this area and a large number of inter-
23 esting results can be found in various journals dedicated to sport, medicine, physics,
24 engineering, etc. Basic theoretical principles are summarised in several monographs
25 (e.g. Howe, 1983; Lind & Sanders, 1996). Although a significant progress has
26 been made, we are still far from the point where researches can declare a complete
27 understanding of the topic and provide a clear guidance to skiing enthusiasts and
28 professionals. The main problem is that a skier and their equipment is a very com-
29 plicated mechanical system with many degrees of freedom. In order to arrive to a
30 treatable and comprehensible mathematical model, a great deal of simplification is
31 required.

32 The most basic approach is to treat the skier as a point mass moving under
33 the action of the gravitational force, the snow reaction forces and the aerodynamic
34 drag (Howe, 1983; Lind & Sanders, 1996). The snow reaction force is known
35 to depend on the angle between the longitudinal axis of skis and their direction of
36 motion, the so-called angle of attack. For example in order to brake and stop, skis
37 are routinely pivoted to the angle of attack about 90° . This force also depends on
38 whether skis are flat on the snow or put at an angle with to it, called the edge angle.
39 For example in order to halt side-slipping down the fall line, skiers increase the edge
40 angle by increasing inclination of their body to the slope and/or its angulation. The
41 inclination angle is also important for the lateral balance of skiers as deviation from
42 the balanced inclination may result in a fall. In fact, in mathematical modelling of
43 skiing it is commonly assumed that during straight runs, traversed runs, and even
44 turns, skier's body is in lateral balance. This dictates the position of their centre of
45 mass (CM) over the skis and hence allows to introduce the ski edge angle into the
46 dynamics of point mass (Howe, 1983; Lind & Sanders, 1996).

47 At the over extreme we find more complex Hanavan-like models of skiers and
48 their equipment, where they are represented by many rigid segments connected by me-
49 chanical joints (Oberegger, Kaps, Mössner, Heinrich, & Nachbauer, 2010). While this
50 approach is undoubtedly very useful in studying the ski-snow interaction (P. Federolf,
51 Roos, Lüthi, & Dual, 2010; Mössner, Heinrich, Kaps, Schretter, & Nachbauer, 2008;
52 Mössner, Heinrich, Kaps, Schretter, & Nachbauer, 2009; Mössner et al., 2006), the
53 biomechanical response of a human body is very complex a hence very difficult to
54 model accurately. It requires a significant element of artificial intelligence. Undoubt-
55 edly, this is the future of computer modelling of skiing, but at the moment more basic
56 models allowing simple interpretation and clear insights into the key factors of skiing
57 dynamics seem more appropriate.

58 The apparently lesser problem of the interaction between skis and snow is also
59 complicated, and not only due to the non-trivial ski construction but also due to the
60 existence of many different types of snow with their complex structure and physics.

61 Even for straight gliding one has to differentiate between the so-called dry friction,
62 which arises in the case of direct contact of the ski base with the snow, and the
63 wet friction, which arises due to meltwater lubrication of the ski base (e.g. Colbeck,
64 1992; Nachbauer, Kaps, Hasler, & Mössner, 2016). In soft fresh snow and slush, the
65 processes of snow compactification and plowing can be the dominant contributors to
66 effective friction (e.g. Colbeck, 1992). On hard snow typical for machine-prepared
67 pistes and race tracks, the snow-ski-edge interaction becomes important. This in-
68 teraction may be analogous to that between a sharp hardened tool and a workpiece
69 in machining operations (Brown, 2009; Merchant, 1945; Tada & Hirano, 2002).
70 Indeed, ski racers meticulously keep the edges of their skis razor-sharp.

71 A modern generic ski turn is hybrid in nature. It is initiated with pivoting
72 skis towards the new turn direction and skidding, and it is finished as carving (e.g.
73 LeMaster, 2010; Reid, 2010; Spörri, Kröll, Gildien, & Müller, 2016). At one
74 extreme end of the distribution of hybrid turns, we have a pure skidded (or steered)
75 turn, where a significant angle of attack is preserved from start to finish. The turning
76 action of this turn arises due to the component of the snow reaction force which is
77 normal to the direction of motion (Hirano, 2006; Nordt, Springer, & Kollár, 1999;
78 Tada & Hirano, 2002). At the other extreme, we find a pure carved turn, where the
79 angle of attack is almost zero and each ski moves along a curved groove it cuts in the
80 snow. The groove curvature is determined by the geometry of the ski edge and the
81 ski edge angle (Howe, 1983; Lind & Sanders, 1996). A simple way of determining
82 the composition of a hybrid turn is via naked eye inspection of the tracks left by the
83 skis on the snow. Where the tracks are wide, the turn is skidded, and where they
84 are narrow, it is carved. The closer tracks are to narrow lines from start to finish
85 the closer the turn is to a purely carved one. In terms of performance, the main
86 advantage of carved turns is significant reduction of energy dissipation and hence
87 increased speed.

88 The advance of modern highly shaped skis has moved the focus of both competi-
89 tive and high-performance recreational skiing from steered to carved turns. Nowadays
90 even mass-produced skis are shaped, thus giving the opportunity to enjoy carving runs
91 to all skiing enthusiasts. This has even made an impact on the way the alpine skiing
92 is taught by some ski instructors, who now teach how to initiate a new turn not via
93 pivoting but by rolling skis from edge to edge (e.g. Harb, 2006).

94 The dynamics of carving turns has already received significant attention in the
95 theory of skiing (Howe, 1983; Jentschura & Fahrbach, 2004; Lind & Sanders, 1996).
96 Naively, one may think that skiers can change the edge angle of their skis at will and
97 hence fully control the local shape (curvature) of their trajectory. However, this is not
98 quite the case because the edge angle is largely dictated by the inclination angle of the
99 skier, which is also an important parameter for skier's lateral balance. For example, a
100 stationary skier must stay more-or-less vertical to avoid falling to the one side or the
101 other. If their whole body is aligned (or "stacked") with the vertical direction then
102 the ski edge angle equals the angle of the slope gradient. If their body is angulated

103 at their knees or hip, while keeping the CM above the skis, the edge angle is different
 104 but this variation is limited in amplitude. A similar analysis of skier's balance during
 105 pure carving turns allows to derive a relatively simple equation which relates the edge
 106 angle and hence the local curvature of skier's trajectory with their speed and direction
 107 of motion relative to the fall line (Howe, 1983; Jentschura & Fahrbach, 2004; Lind
 108 & Sanders, 1996). This so-called Ideal Carving Equation (ICE) removes the need
 109 for specifying the component of the snow reaction force responsible for the turning
 110 action, which is a significant gain. As a result, the motion of skiers's CM can be fully
 111 determined in a model where only the gravity, dynamic friction and air resistance
 112 forces are explicitly taken into account.

113 Testing the hypothesis that this simplified model adequately describes the dy-
 114 namics of carving turns is the main topic of this paper. In particular, Jentschura and
 115 Fahrbach (2004) discovered an upper limit on the skier speed imposed by ICE. They
 116 concluded that in slalom races the typical speed is below this limit and considered
 117 this as a justification of the model. By calculating the actual motion of a skier as
 118 governed by this model, one can trace the evolution of their speed and check the
 119 conditions under which it stays below the limit. This can be done not only for slalom
 120 but also for other race disciplines.

121 Methods

122 The characteristic scales of fall-line gliding

123 Although recreational skiing can be very relaxed and performance skiing phys-
 124 ically most demanding, the dominant source of energy in both cases is the Earth's
 125 gravity. The total available gravitational energy is

$$U = mgh, \quad (1)$$

126 where m is skier's mass, g is the gravitational acceleration and h is the total vertical
 127 drop of the slope. If all this energy was converted into the kinetic energy of the skier,
 128 $K = mv^2/2$, then at the bottom of the slope the speed would reach

$$v = \sqrt{2gh} \approx 227 \left(\frac{h}{200 \text{ m}} \right)^{1/2} \text{ km/h}. \quad (2)$$

129 Although this not far from what is achieved in the speed skiing competitions where
 130 skiers glide straight down the fall line, the typical speeds in other alpine disciplines
 131 are significantly lower, indicating there are some forces working against gravity. Two
 132 of the candidates are the dynamic snow friction and the aerodynamic drag (Lind &
 133 Sanders, 1996).

134 The friction force is antiparallel to the skier velocity vector \mathbf{v} and its magnitude
 135 relates to the normal reaction force \mathbf{F}_n . Although the physics of snow friction is quite
 136 complicated (e.g. Lind & Sanders, 1996), the basic Coulomb equation

$$F_f = \mu F_n, \quad (3)$$

137 is almost universally used both in describing the results of field studies and in mod-
 138 elling of ski runs (e.g. Lind & Sanders, 1996; Mössner et al., 2008; Nachbauer et
 139 al., 2016; Rudakov, Lisovski, Ilyalov, & Podgaets, 2010). The dynamic coefficient
 140 of friction μ depends on many factors, e.g. snow temperature, wax used and even
 141 the value of F_n , making the relation between F_f and F_n nonlinear (e.g. Nachbauer et
 142 al., 2016). Sometimes, even the effect of snowplowing in a skidded turn is described
 143 using the Coulomb law (Sahashi & Ichino, 1998), leading to very high values of the
 144 coefficient $\mu \leq 0.3$. For the purpose of our study it is sufficient to use constant μ and
 145 to address how its value affects the outcome of simulations.

146 In the case of gliding down the fall line

$$F_n = mg \cos \alpha, \quad (4)$$

147 where α is the angle between the slope and the horizontal plane. Because the friction
 148 force does not depend on the skier's speed, it cannot limit the speed but only reduces
 149 its growth rate. The aerodynamic drag force is also antiparallel to the velocity vector
 150 and has the magnitude

$$F_d = \kappa v^2 \quad \text{where} \quad \kappa = \frac{C_d A \rho}{2}, \quad (5)$$

151 where C_d is the drag coefficient, A is the cross-section area of the skier normal to
 152 the direction of motion and ρ is the mass density of the air (Lind & Sanders, 1996).
 153 The drag force grows with v and this results in speed saturation. The value of the
 154 saturation speed v_s can be easily found from the energy principle. At this speed, the
 155 work carried out by the drag and friction forces over the distance L along the fall
 156 line,

$$W = (F_f + F_d)L, \quad (6)$$

157 must be equal to the gravitational energy $U = mgh$ released over the same distance.
 158 This condition yields

$$v_s^2 = \frac{mg}{\kappa} \sin \alpha (1 - \mu \cot \alpha) \quad (7)$$

159 (cf. Lind and Sanders (1996)). Incidentally, this result shows that the slope angle has
 160 to exceed $\alpha_{\min} = \arctan(\mu)$. For the realistic value $\mu = 0.04$ (Lind & Sanders, 1996),
 161 this gives $\alpha_{\min} = 2.3^\circ$. Usually ski slopes are significantly steeper than this and the
 162 snow friction contribution is small. In this case, the saturation speed is determined
 163 mostly by the balance between the gravity and aerodynamic drag, which yields the
 164 characteristic speed scale

$$V_g = \sqrt{\frac{mg}{\kappa} \sin \alpha}. \quad (8)$$

165 The time required to reach this speed under the action of gravity alone,

$$T_g = \frac{V_g}{g \sin \alpha} = \sqrt{\frac{m}{\kappa g \sin \alpha}}, \quad (9)$$

166 is the corresponding characteristic time scale. The length scale

$$L_g = \frac{V_g T_g}{2} = \frac{m}{2\kappa} \quad (10)$$

167 is the corresponding distance along the slope. Interestingly, L_g does not depend on
 168 the slope gradient, which may not be very intuitive. Lind and Sanders (1996) state
 169 the values $C_d = 0.5$, $m = 80$ kg, $A = 0.4$ m², and $\rho = 1.2$ kg/m³ as typical for downhill
 170 (DH) competitions. For these parameters

$$V_g \simeq 150 \sqrt{\frac{\sin \alpha}{\sin 15^\circ}} \text{ km/h}, \quad T_g \simeq 16 \sqrt{\frac{\sin 15^\circ}{\sin \alpha}} \text{ s}, \quad L_g \simeq 0.33 \text{ km}. \quad (11)$$

171 These scales are well below the lengths of race tracks and durations of ski runs in all
 172 alpine disciplines, suggesting that V_g can be reached in all of them. For example, the
 173 length of Kitzbuhel's famous DH track Streif is 3.3km ($\langle \alpha \rangle = 15^\circ$) and the length of it
 174 slalom track Ganslern is 0.59km ($\langle \alpha \rangle = 19^\circ$) (www.hahnenkamm.com). Although on
 175 some sections of downhill (DH) courses the skier speed can indeed approach V_g , with
 176 the current record of 162 km/h belonging to Johan Clarey (FIS WC race in Wengen,
 177 2013), the typical mean speed in DH is $\langle v \rangle \simeq 90$ km/h, which is significantly lower
 178 than V_g (e.g. Gilgien, Spörri, Kröll, Crivelli, & Müller, 2014). In slalom (SL) it stays
 179 well below, only 40 – 50 km/h (e.g. Reid, 2010; Supej, Hebert-Losier, & Holmberg,
 180 2014), indicating that the applicability of the fall-line gliding model is rather limited.
 181 In equation (11) we used $\alpha = 15^\circ$ as a typical mean gradient of red slopes. On steeper
 182 slopes, the limitation of the model is even more pronounced.

183 Basic dynamics of alpine skiing

184 Here we limit ourselves to the idealised case of a plane slope with constant
 185 gradient and introduce such system of Cartesian coordinates $\{x, y, z\}$ associated with
 186 the slope that on its surface $z = 0$. The unit vectors parallel to the coordinate
 187 axes will be denoted as $\{\mathbf{i}, \mathbf{j}, \mathbf{k}\}$ respectively. For convenience, we direct the y-axis
 188 along the fall line, pointing downhill. We also introduce the vertical unit vector
 189 $\mathbf{s} = -\sin(\alpha)\mathbf{j} + \cos(\alpha)\mathbf{k}$, so that the gravitational acceleration $\mathbf{g} = -g\mathbf{s}$ (see figure
 190 1).

191 When only the gravity, normal reaction, dynamic friction and aerodynamic drag
 192 forces are taken into account, the second law of Newtonian mechanics governing the
 193 motion of skier's centre of mass (CM) reads

$$m \frac{d\mathbf{v}}{dt} = \mathbf{F}_g + \mathbf{F}_f + \mathbf{F}_d + \mathbf{F}_n, \quad (12)$$

194 where

$$\mathbf{F}_g = m\mathbf{g}, \quad \mathbf{F}_f = -\mu F_n \mathbf{u}, \quad \mathbf{F}_d = -kv^2 \mathbf{u} \quad (13)$$

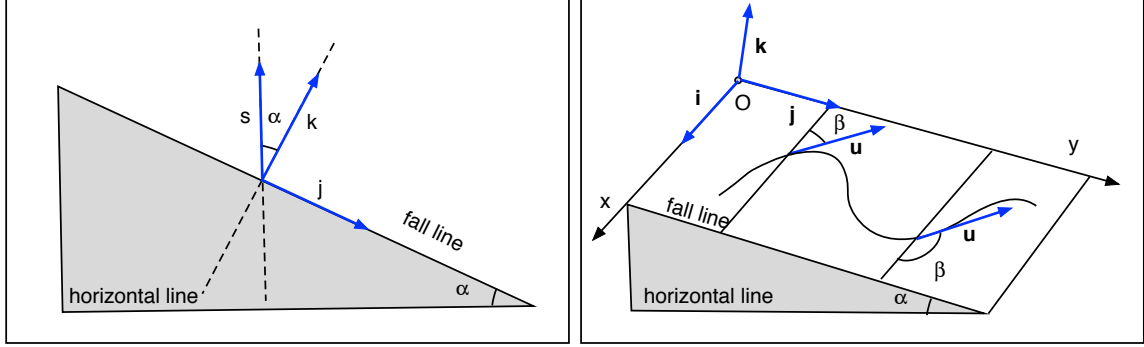


Figure 1. Geometry of the slope. *Left panel:* The vertical section of the slope along the fall line. *Right panel:* The slope as seen at an angle from above. The curved line in the middle is the skier trajectory.

195 are the total gravity, friction, aerodynamic drag, and snow reaction force acting on
 196 the skier, respectively, and \mathbf{F}_n is the normal reaction. In these expressions, \mathbf{u} is the
 197 unit vector in the direction of motion. It is convenient to introduce the *angle of*
 198 *traverse* β as the angle between $-\mathbf{i}$ and \mathbf{u} for the right turns and between \mathbf{i} and \mathbf{u}
 199 for the left turns of a run (see figure 1). With this definition,

$$\mathbf{u} = \mp \cos(\beta)\mathbf{i} + \sin(\beta)\mathbf{j} \quad (14)$$

200 where the upper sign of $\cos \beta$ corresponds to the right turns and the lower sign to the
 201 left turns (we will use this convention throughout the paper).

202 The normal reaction force \mathbf{F}_n is not as easy to describe as the other forces.
 203 First, unless the skis are running flat on the slope, this force is normal not to the
 204 slope surface but to the contact surface between the snow and the skis, which is not
 205 the same thing. When skis are put on edge, they carve a platform (or a step) in the
 206 snow and the normal reaction force is normal to the surface (surfaces) of this platform
 207 (LeMaster, 2010). Second, the effective weight of the skier is determined not only by
 208 the gravity but also by the centrifugal force, which depends on the skier speed and
 209 the local curvature of their trajectory.

210 Since the velocity vector $\mathbf{v} = v\mathbf{u}$ we have

$$\frac{d\mathbf{v}}{dt} = \mathbf{u}\frac{dv}{dt} + v\frac{d\mathbf{u}}{dt}. \quad (15)$$

211 Ignoring the up and down motion of CM, we can write $d\mathbf{u}/dt = \mathbf{c}|d\beta/dt|$, where \mathbf{c} is
 212 the centripetal unit vector which points towards the local centre of curvature of the
 213 CM trajectory. Hence,

$$\frac{d\mathbf{v}}{dt} = \mathbf{u}\frac{dv}{dt} + v\mathbf{c}\left|\frac{d\beta}{dt}\right|. \quad (16)$$

214 Since $dt = dl/v$, where l is the distance measured along the skier trajectory, the last
 215 equation can also be written as

$$\frac{d\mathbf{v}}{dt} = \mathbf{u} \frac{dv}{dt} + \frac{v^2}{R} \mathbf{c}, \quad (17)$$

216 where

$$R = \left| \frac{dl}{d\beta} \right| \quad (18)$$

217 is the (local) radius of curvature of the trajectory. Hence, we can rewrite equation
 218 (12) as

$$m\mathbf{u} \frac{dv}{dt} + \frac{mv^2}{R} \mathbf{c} = \mathbf{F}_g + \mathbf{F}_f + \mathbf{F}_d + \mathbf{F}_n. \quad (19)$$

219 Scalar multiplication of equation (19) with \mathbf{u} delivers the equation governing
 220 the evolution of skier's speed. Since $\mathbf{u} \cdot \mathbf{c} = 0$, $\mathbf{u} \cdot \mathbf{u} = 1$, $\mathbf{u} \cdot \mathbf{s} = -\sin \alpha \sin \beta$,
 221 this equation reads

$$\frac{dv}{dt} = g \sin \alpha \sin \beta - \mu \frac{F_n}{m} - \frac{k}{m} v^2. \quad (20)$$

222 The normal reaction force can be decomposed into components parallel to \mathbf{c} and
 223 \mathbf{k} :

$$\mathbf{F}_n = F_{n,c} \mathbf{c} + F_{n,k} \mathbf{k}. \quad (21)$$

224 The scalar multiplication of equation (19) and \mathbf{k} immediately yields

$$F_{n,k} = mg \cos \alpha. \quad (22)$$

225 Thus, the normal to the slope component of the snow reaction force \mathbf{F}_n is the same
 226 as in the case of the fall-line gliding. This is what is needed to match exactly the
 227 normal to the slope component of the gravity force and hence to keep the skier on
 228 the slope.

229 Since $\mathbf{c} = \pm \sin(\beta) \mathbf{i} + \cos(\beta) \mathbf{j}$, (see figure 2) and hence $(\mathbf{s} \cdot \mathbf{c}) = -\sin \alpha \cos \beta$,
 230 the scalar multiplication of equation (19) with \mathbf{c} yields

$$F_{n,c} = \frac{mv^2}{R} - mg \sin \alpha \cos \beta. \quad (23)$$

231 This component of the normal reaction force is stronger in the lower-c part of the
 232 turn ($90^\circ < \beta < 180^\circ$), where the angle between the gravity force and the centrifugal
 233 force is less than 90° , and weaker in the upper-c part of the turn ($0^\circ < \beta < 90^\circ$),
 234 where this angle is more than 90° (the terminology is from Harb (2006)).

235 The total strength of \mathbf{F}_n (and hence the effective weight of the skier) is

$$F_n = \frac{mg \cos \alpha}{\cos \Phi}, \quad (24)$$

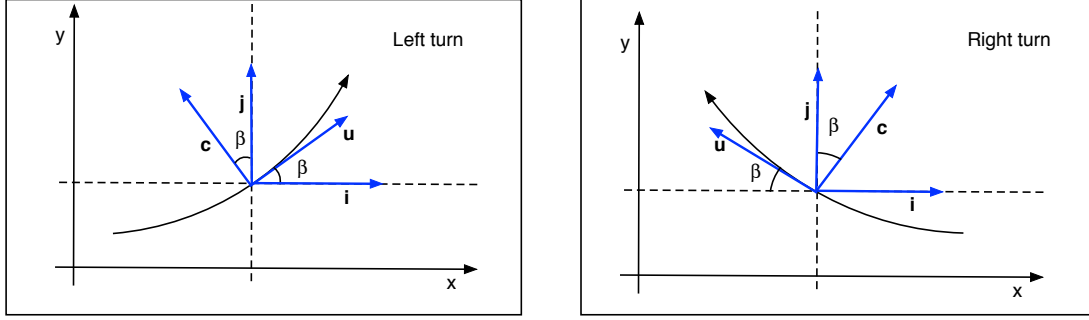


Figure 2. The centripetal unit vector \mathbf{c} for left and right turns.

236 where Φ is the angle between \mathbf{F}_n and the normal direction to the slope \mathbf{k} , given by

$$\tan \Phi = \frac{F_{n,c}}{F_{n,k}} = \frac{v^2}{gR} \frac{1}{\cos \alpha} - \tan \alpha \cos \beta. \quad (25)$$

237 In the case of fall-line gliding, $\Phi = 0^\circ$ and this equation reduces to the familiar
238 $F_n = mg \cos \alpha$, as expected.

239 Formally, equations (22,23) can be written as one vector equation

$$\mathbf{F}_n + \mathbf{F}_c + \mathbf{F}_{g,\text{lat}} = 0, \quad (26)$$

240 where

$$\mathbf{F}_{g,\text{lat}} = -(mg \cos \alpha)\mathbf{k} + (mg \sin \alpha \cos \beta)\mathbf{c} \quad (27)$$

241 is the lateral (normal to \mathbf{u}) component of the gravity force and

$$\mathbf{F}_c = -(mv^2/R)\mathbf{c} \quad (28)$$

242 is the centrifugal force. Equation (26) also holds in the accelerated (non-inertial)
243 frame of the skier where \mathbf{F}_c emerges as an inertial force. In this frame, the skier is at
244 rest and equation (26) has the meaning of lateral force balance. As any inertial force,
245 the centrifugal force has the same properties as the gravity force and their sum plays
246 the role of effective gravity experienced by the skier. Introducing the lateral effective
247 gravity

$$\mathbf{F}_{g,\text{eff}} = \mathbf{F}_{g,\text{lat}} + \mathbf{F}_c, \quad (29)$$

248 equation (26) can be written as

$$\mathbf{F}_n + \mathbf{F}_{g,\text{eff}} = 0. \quad (30)$$

249 The effective weight F_n is often measured in the units of the standard weight
250 mg , in which case it is also called the g-force. Using equation (24), we find

$$\text{g-force} = \frac{\cos \alpha}{\cos \Phi}. \quad (31)$$

251 The expressions (24,25) for the strength and direction of \mathbf{F}_n do not allow to close
252 the system. Indeed, they involve the turn radius R which still remains undetermined.

253 Radius of balanced carving turn

254 In the mechanics of solid bodies, by a balance we understand not only vanishing
 255 combined (total) force but also vanishing combined torque (Landau & Lifshitz, 1969).
 256 Although skiers are not exactly solid bodies, torques are still important in their
 257 dynamics. Here we focus on the lateral balance of skiers, that is the balance in the
 258 plane normal to the skier speed (the so-called frontal plane; LeMaster, 2010). The
 259 two forces parallel to this plane are the effective gravity $\mathbf{F}_{g,\text{eff}}$ and the normal reaction
 260 \mathbf{F}_n . The effective gravity is applied directly at the CM, whereas the normal reaction
 261 force is applied at the skis and most of it originates from the inside edge of the outside
 262 (relative to the turn arc) ski (LeMaster, 2010). Hence, the condition of vanishing
 263 torque implies that both $\mathbf{F}_{g,\text{eff}}$ and \mathbf{F}_n must act along the line connecting CM with
 264 the inside edge of the outside ski (see figure 3). In other words, the angle between
 265 this line, which we will refer to as the lever arm, and the slope normal, which is called
 266 the skier inclination angle, must be equal to the angle Φ given by equation (25).

267 As a first step, here we focus on the case where the skier is “stacked”, which
 268 means that in the frontal plane their legs are aligned with their torso in the frontal
 269 plane. In this case, skier’s CM is located about their belly button and the lever arm
 270 is normal to the ski base, provided skier’s boots are properly adjusted (the so-called
 271 canting of ski boots; LeMaster, 2010). Hence, the angle Ψ between the ski base
 272 and the slope, which we will call the ski edge angle (see figure 3), equals the skier
 273 inclination angle

$$\Psi = \Phi. \quad (32)$$

274 The running edge of a flattened carving ski is close to an arc of a circle. The
 275 radius of this circle is called the ski sidecut radius, R_{sc} . When the ski is placed at
 276 the edge angle Ψ to a hard flat surface and then pressed in the middle so it bends
 277 and comes into contact with the surface, its edge can still be approximated as an arc
 278 but of a smaller radius

$$R_e = R_{\text{sc}} \cos \Psi \quad (33)$$

279 (Howe (1983), Lind and Sanders (1996), and Appendix A). In pure carving turns,
 280 there is no side-slippage (skidding) and the ski is transported along the contact edge.
 281 This makes the edge curvature radius R_e the same as the local curvature radius of
 282 the ski trajectory.

283 Strictly speaking, this relation is based on the assumption that the penetration
 284 of snow surface by skis is negligibly small, which is best satisfied on an icy race track.
 285 If however the snow is soft, and hence the penetration is significant, it is important
 286 to know how the penetration depth is distributed along the ski. As the pressure
 287 distribution normally peaks under skier’s foot, one may expect the penetration to
 288 be deepest near the ski midpoint. Assuming that both the tip and the tail ends of
 289 the running edge remain on the surface, Howe (1983) derived a modified version of
 290 equation (33), which includes the penetration depth as a parameter and leads to a

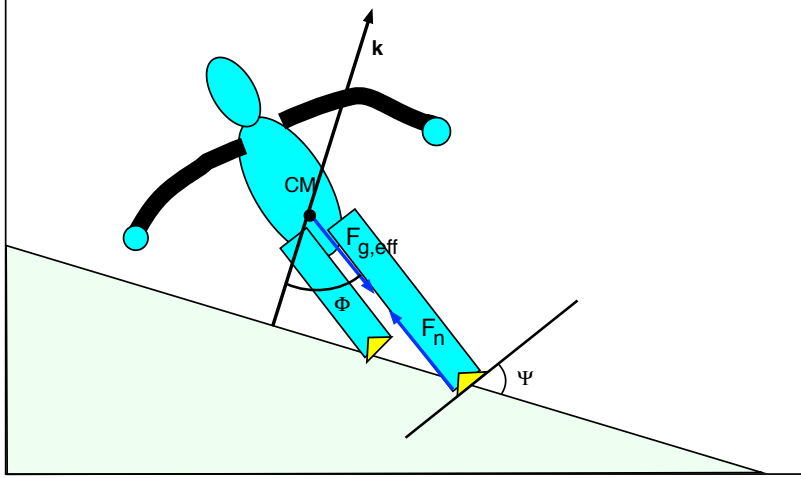


Figure 3. Lateral balance of a stacked (un-angulated) skier. The normal reaction force F_n and the effective gravity force $F_{g,eff}$ act along the line connecting CM with the inside edge of the outside ski, which results in vanishing torque. The skier inclination angle Φ is the same as the ski edge angle Ψ . This configuration corresponds to the lower-c part of the turn.

291 smaller value for R_e . From the basic geometry of the problem it follows that the
 292 effect is significant when the width of the groove platform, on which the ski is resting,
 293 becomes comparable to the ski sidecut h_{SC} , which is about 20 mm for a slalom ski.
 294 Although his analysis is fine for a stationary ski, the snow plasticity ensures that
 295 the ski tail does not return to the surface but instead glides over the platform made
 296 in the snow by the forebody of the ski, thus leading to a higher radius than that
 297 predicted by the modified Howe equation. Moreover, the finite-element model of
 298 the ski-snow interaction by M. Federolf, Lüthi, Roos, and Dual (2010) predicted the
 299 turn radius which for $\Psi > 50^\circ$ was even larger than that given by Howe's formula
 300 with zero penetration. They speculated that this was due to the higher local sidecut
 301 radius of the ski afterbody. To the contrary, in the field study of turns performed by
 302 members of the Norwegian national team, Reid, Haugen, Gilgien, Kipp, and Smith
 303 (2020) found a good agreement with equation (33) up to $\Psi \simeq 70^\circ$.

304 A differential twisting (torsion) of the ski about its longitudinal axis, leading to
 305 lower value of Ψ at its tip and tail compared to the mid-ski position, increases R_e .
 306 However, this effect is likely to be marginal. Yoneyama, Scott, Kagawa, and Osada
 307 (2008) measured the deflection angle at the ski tip during a ski run to be $\delta\Psi \leq 2^\circ$
 308 and concluded that it had little effect on the geometry of the running edge. Indeed,
 309 the effective sidecut of the edge is reduced by $\delta h \simeq d(1 - \cos \delta\Psi)$, where d is the
 310 half-width of the ski at the tip. Even for $\delta\Psi$ as high as 10° and $d = 60$ mm this leads
 311 to $\delta h \approx 0.9$ mm.

312 Obviously, the applicability of Howe’s formula (33) has to be clarified. In our
 313 study we adopt it, keeping in mind that it may be sufficiently accurate only for icy
 314 snow.

315 The ski trajectory is not the same as the CM trajectory. It is longer and
 316 in general has higher curvature (e.g. LeMaster, 2010), and so $R > R_e$. This is
 317 particularly pronounced in short slalom turns (e.g. Reid, 2010; Supej et al., 2014).
 318 However, the separation between the trajectories is limited by the length of skier
 319 leg and for sufficiently wide turns we may assume that $R \approx R_e$. Hence, combining
 320 equations (33) and (25) with the balance condition $\Phi = \Psi$, we find

$$\left(\left(\frac{R_{sc}}{R} \right)^2 - 1 \right)^{1/2} = \frac{v^2}{gR \cos \alpha} - \tan \alpha \cos \beta. \quad (34)$$

321 This is a different form of equation (10-1) in Howe (1983) and it is called by Jentschura
 322 and Fahrbach (2004) the Ideal-Carving Equation (ICE). It defines R as a function of
 323 skier’s velocity and therefore allows to close the CM equations of motion.

324 According to equation (33), R is a monotonically decreasing function of Ψ . It is
 325 easy to see that $R \rightarrow R_{sc}$ as $\Psi \rightarrow 0$ and hence the turn radius of marginally edged ski
 326 is about R_{sc} . At the other end of the range, $R \rightarrow 0$ as $\Psi \rightarrow 90^\circ$, which does not make
 327 much sense and reflects the approximate nature of (33). Obviously, there is a limit
 328 to how much a ski can be bent before it breaks. If $r_b = R/l_{ski}$ is the radius of ski
 329 curvature at the breaking point measured in ski lengths, then we have the constraint
 330 $\cos \Phi > r_b(l_{ski}/R_{sc})$. For a slalom ski with $l_{ski} = 1.65$ m and $R_{sc} = 13$ m and the
 331 fairly reasonable $r_b = 2$, this yields the condition on the ski edge angle $\Psi < 75^\circ$.

332 Another upper limit is set by the g-force which builds up during the turn.
 333 According to LeMaster (2010) the best athletes can sustain the g-force up to about
 334 three. According to equation (31), this leads to the condition $\Phi < 70^\circ$ (for the realistic
 335 slope gradient angle $\alpha = 15^\circ$).

336 Finally, as Φ increases so does the tangential to the slope component of the
 337 effective gravity. This is effectively a shearing force acting on the snow. Above a
 338 certain level it will cause snow fracturing, loss of grip and skidding (Mössner et al.,
 339 2009; Mössner et al., 2013). The snow shear stress S relates to $F_{n,c}$ via

$$F_{n,c} = l_{ski} e S, \quad (35)$$

340 where e is the snow penetration depth in the direction normal to the slope. The
 341 snow fractures when the shear stress exceeds the critical value S_c . Based on equation
 342 (35) alone one might naively expect that S_c sets a lower limit on the snow penetra-
 343 tion. However, this ignores the fact that the penetration is dictated by the normal
 344 component $F_{n,k}$ of the same force. These are related via

$$F_{n,k} = HV, \quad (36)$$

345 where $V = l_{\text{ski}} e^2 / 2 \tan \Psi$ is the volume of the imprint made by the ski in the snow
 346 and H is the hardness parameter of the snow (Mössner et al., 2013). Combining
 347 equations (35,36,32) one finds

$$e < \frac{2S_c}{H}, \quad (37)$$

which is an upper limit on the penetration, contrary to the naive expectation. This can be turned into the condition on the skier inclination angle. Indeed, using equations (22,32,36) one finds

$$e^2 = \frac{2mg \cos \alpha \tan \Phi}{H l_{\text{ski}}}$$

348 and, upon the substitution of this result into equation (37), the condition

$$\tan \Phi < \frac{2S_c^2 l_{\text{ski}}}{mgH \cos \alpha}. \quad (38)$$

349 According to the analysis in Mössner et al. (2013), a well-prepared race track can be
 350 attributed with $S_{\text{cr}} \approx 0.52 \text{ N mm}^{-2}$ and $H \approx 0.21 \text{ N mm}^{-3}$. Using these values along
 351 with $m = 70 \text{ kg}$, $l_{\text{ski}} = 165 \text{ cm}$ and $\alpha = 15^\circ$ we obtain $e < 5 \text{ mm}$ and $\Phi < 81^\circ$. Thus,
 352 all three conditions yield approximately the same upper limit on Φ .

353 Looser snow will fracture under much lower shear stress, thus allowing only
 354 small-inclination carving. For example, in their sophisticated multi-body simula-
 355 tions, which incorporated a multi-segment ski model, Mössner et al. (2008) used
 356 $H = 0.01 \text{ N mm}^{-3}$ and $S_{\text{cr}} = 0.03 \text{ N mm}^{-2}$ and observed a transition to skidding dur-
 357 ing the very first turn. As the turn progressed, the inclination angle of effective gravity
 358 increased from $\Phi = 0^\circ$ to $\Phi \approx 45^\circ$. For these snow parameters, $l_{\text{ski}} = 165 \text{ cm}$ and
 359 $m = 72 \text{ kg}$, used in their simulations, equation (38) yields the critical angle $\Phi_c = 24^\circ$,
 360 which is consistent with the simulation results.

361 Speed limits imposed by the Ideal Carving Equation

362 Equation (34) can be written as

$$(\xi^2 - 1)^{1/2} = a\xi + b, \quad (39)$$

363 where $\xi = R_{\text{sc}}/R$, $a = v^2/gR_{\text{sc}} \cos \alpha$ and $b = -\cos \beta \tan \alpha$. From the definitions
 364 it follows that $\xi \geq 1$, $a > 0$ and $|b| < \tan \alpha$. The right-hand side of (39) is the
 365 linear function $g(\xi) \equiv \tan \Psi(\xi) = a\xi + b$ which monotonically increases with ξ . The
 366 left-hand side of (39) is the radical function $f(\xi) \equiv \tan \Phi(\xi) = \sqrt{\xi^2 - 1}$ which also
 367 monotonically increases with ξ . Moreover, since $f'' = -1/\sqrt{\xi^2 - 1} < 0$, f' decreases
 368 monotonically from $+\infty$ at $\xi = 1$ to 1 as $\xi \rightarrow +\infty$.

369 Whether the solutions to (39) exist or not critically depends on whether $a < 1$
 370 or $a > 1$. The critical value $a = 1$ corresponds to $v = V_{\text{sc}}$ where

$$V_{\text{sc}} = \sqrt{gR_{\text{sc}} \cos \alpha} \quad (40)$$

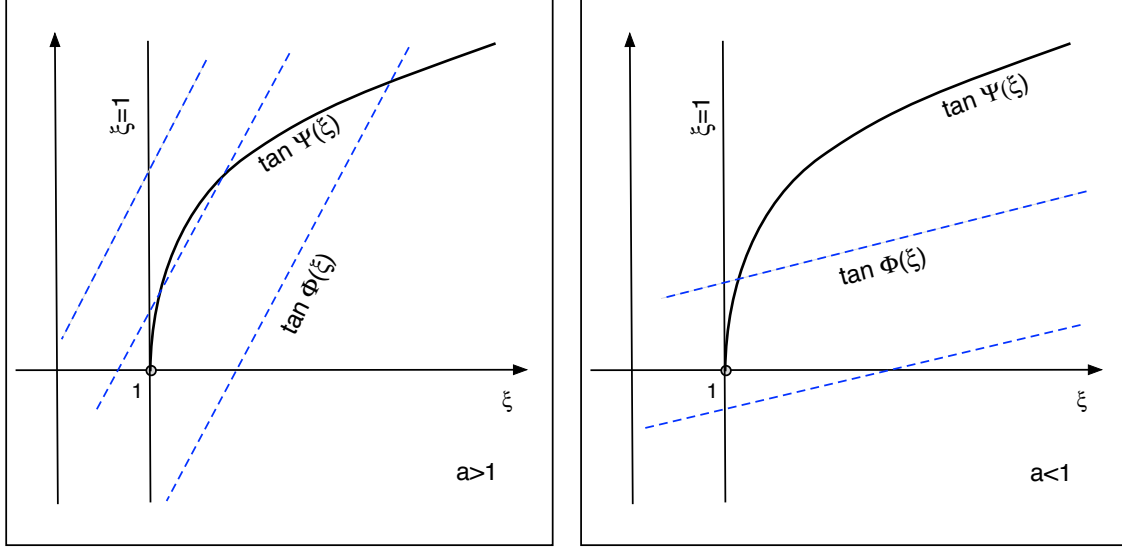


Figure 4. Finding roots of the ideal carving equation (ICE). The solid line shows $\tan \Psi(\xi) = \sqrt{\xi^2 - 1}$ and the dashed lines $\tan \Phi(\xi) = a\xi + b$. The roots of ICE are given by the intersection points of the curves. *Left panel:* The case $a > 1$. Depending on the value of b , one can have none, one or two roots. *Right panel:* The case $0 < a < 1$. Now one can have either one root or none.

371 (cf. Jentschura & Fahrbach, 2004).

372 When $a < 1$ ($v < V_{sc}$), the gradient of $g(\xi)$ is lower than the asymptotic gradient
 373 of $f(\xi)$ and as illustrated in the right panel of figure 4 there is either one solution
 374 or none. The solution exists when $a + b \geq 0$, which includes the case of $b > 0$ and
 375 hence there is always a unique solution for the lower-c part of the turn. This solution
 376 disappears when $a + b < 0$ which implies negative b and hence the upper-c part of the
 377 turn. In terms of the turn speed and the angle between the skier velocity and the
 378 fall line, $\gamma = |\beta - 90^\circ|$, the existence condition reads

$$\sin \gamma \leq \frac{v^2}{gR_{sc} \sin \alpha}. \quad (41)$$

Thus, for sufficiently low speeds, namely $v^2 < gR_{sc} \sin \alpha$, carving is possible only close to the fall line. In order to understand this result, consider a stationary skier whose skis point perpendicular to the fall line. In order to stay in balance the skier has to be aligned with the vertical direction and this implies ski edging which is consistent with the lower-c part of the turn only. Hence, if the skier is pushed forward just a little bit then their trajectory will turn not downhill but uphill. To turn downhill the skis must be at least flat on the snow (or marginally edged) in which case they carve an arc of the radius $R = R_{sc}$. The balance condition (26) then implies that the corresponding centrifugal force mv^2/R_{sc} must be high enough to balance the centripetal component

of the gravity force $mg \sin \alpha \cos \beta$. This yields the speed

$$v^2 = gR_{sc} \sin \alpha \sin \gamma,$$

379 in agreement with condition (41).

When $a > 1$ ($v > V_{sc}$), the gradient of $g(\xi)$ is higher than the asymptotic gradient of $f(\xi)$ and as one can see in the left panel of figure 4 there are three distinct possibilities. If $g(1) = a + b < 0$ then there exists one and only one root. As we increase b above $-a$, then initially there are two roots but eventually they merge and disappear. The bifurcation occurs at the point ξ_c where

$$g(\xi_c) = f(\xi_c) \quad \text{and} \quad g'(\xi_c) = f'(\xi_c).$$

380 Solving these two simultaneous equations for ξ_c and b_c , we find that

$$b_c = -(a^2 - 1)^{1/2} \quad \text{and} \quad \xi_c = \frac{a}{(a^2 - 1)^{1/2}}. \quad (42)$$

381 There are no solutions when $b > b_c$, which includes all positive values of b and hence
382 the whole lower-c part of the turn. This means that at such high speeds balanced
383 carving turns are impossible.

What are the indications that a skier is about to hit the speed limit V_{sc} ? Consider the entrance point to the lower-c part of the turn. At this point $\beta = 90^\circ$, $b = 0$ and hence equation (39) reads

$$(\xi^2 - 1)^{1/2} = a\xi.$$

Its solution

$$\xi = \frac{1}{\sqrt{1 - a^2}} \rightarrow \infty \quad \text{as} \quad a \rightarrow 1.$$

Thus the turn becomes very tight (formally $R \rightarrow 0$) and the skier's body close to horizontal (formally $\Phi \rightarrow 90^\circ$). On approach to this point something will give up. As we discussed earlier this will be either the skis, the skier's legs or the snow resistance to the applied shearing force. If however the speed limit is exceeded in the upper-c part of the turn, there may not be such a clear indicator. In fact, after this the turn can be continued for a while until it reaches the critical traverse angle β_c where

$$\cos \beta_c = \cot \alpha \left(\left(\frac{v}{V_{sc}} \right)^4 - 1 \right)^{1/2}$$

384 and

$$\tan \Phi_c = \left(\left(\frac{v}{V_{sc}} \right)^4 - 1 \right)^{-1/2} \quad (43)$$

385 (see equations 42). When v grows slowly at the point of going over V_{sc} , the loss
386 of balance occurs close to the fall line at extreme inclination angles. If however the

387 growth is fast, v may significantly overshoot V_{sc} quite early in the upper-c part of
 388 turn. In this case the loss of balance may also occur early and at Φ significantly below
 389 90° .

390 Figure 4 shows that when $v > V_{sc}$ no balanced position exists because for any
 391 turn radius $\Phi > \Psi$. The effective gravity is not directed along the lever arm but
 392 points away from it, resulting in non-vanishing net torque about the point where the
 393 carving ski is “pinned” to the snow. This torque pushes the skier body away from
 394 the slope towards the position with zero inclination.

395 It is easy to show that

$$V_{sc} = V_g \left(\frac{R_{sc}}{L_g \tan \alpha} \right)^{1/2}. \quad (44)$$

396 For the typical parameters of slalom competitions, this gives

$$V_{sc} = 0.3V_g \left(\frac{R_{sc}}{13 \text{ m}} \right)^{1/2} \left(\frac{L_g}{200 \text{ m}} \right)^{-1/2} \left(\frac{\tan \alpha}{\tan 20^\circ} \right)^{-1/2}. \quad (45)$$

397 Thus, for carving turns in slalom V_{sc} is significantly smaller than the characteristic
 398 speed V_g (see equation 8) set by the aerodynamic drag. This suggests that pure carv-
 399 ing turns are normally impossible for the typical parameters of slalom competitions
 400 and the racers have to shave their speed via skidding on a regular basis. The only
 401 exceptions are probably (i) low gradient sections of the track where the last factor
 402 of equation (45) can be sufficiently large, (ii) the first few turns right after the start,
 403 where the speed has not yet approached V_{sc} and (iii) the few turns at the transitions
 404 from steep to flat part of the race track. In the last case, V_{sc} significantly increases
 405 at the transition, giving to the racer the opportunity to increase their speed as well.
 406 It is easy to verify that the situation is quite similar in other race disciplines.

407 Stability

408 The equilibrium of a stacked skier who keeps all the load on the outside ski
 409 is similar to that of an inverted pendulum and hence unstable (Lind and Sanders
 410 (1996), Appendix B). However, skiers have ways of controlling this instability. Lind
 411 and Sanders (1996) discuss the stabilising arm moment, similar to what is used by
 412 trapeze artists. Ski poles can provide additional points of support when planted into
 413 or dragged against the snow. Some control can be provided by the body angulation
 414 (Appendix B). Finally and presumably most importantly, when both skis are suffi-
 415 ciently wide apart and loaded, instead of the unique balanced inclination angle we
 416 have a continuum of balanced positions (see Appendix B) and so small perturbations
 417 just shift the skier to nearby equilibria. Moreover, this gives to skiers a simple way
 418 of controlling their inclination angle – via relaxing and extending their legs.

419 **Dimensionless equations of carving turn**

It is common practice of mathematical modelling to operate with dimensionless equations, which are derived using a set of scales characteristic to the problem under consideration, instead of standard units. This leads to simpler equations which are easier to interpret and to the results which are at least partly scale-independent. Since in ideal balanced carving the speed must stay below V_{sc} this is a natural speed scale. Because the turn radius is limited by R_{sc} this is a convenient length scale. The corresponding time scale is $T_{sc} = R_{sc}/V_{sc}$. In order to derive the dimensionless equations of balanced carving we now write

$$v = V_{sc}\tilde{v}, \quad t = T_{sc}\tilde{t}, \quad R = L_{sc}\tilde{R},$$

420 substitute these into the dimensional equations and where possible remove common
 421 dimensional factors. Finally, we ignore tilde in the notation. In other words, we do
 422 the substitutions $v \rightarrow V_{sc}v$, $t \rightarrow T_{sc}t$, $R \rightarrow R_{sc}R$ and then simplify the results. For
 423 example, the substitution $v \rightarrow V_{sc}v$ into the equation (7) gives the dimensionless
 424 equation for the saturation speed of fall-line gliding

$$v_s = Sr\sqrt{1 - \mu \cot \alpha}, \quad (46)$$

425 which includes the dimensionless speed parameter $Sr = V_g/V_{sc}$. Similarly, we deal
 426 with other dimensional variables should they appear in the equations, e.g. $x \rightarrow R_{sc}x$
 427 and $y \rightarrow R_{sc}y$. In particular, the application of this procedure to (20) gives the
 428 dimensionless speed equation

$$\frac{dv}{dt} = \sin \beta \tan \alpha - \frac{\mu}{R} - Kv^2, \quad (47)$$

429 where

$$K = \frac{R_{sc}}{L_g}, \quad (48)$$

430 is a dimensionless parameter which we will call the dynamic sidecut parameter. The
 431 g-force can be written as

$$\text{g-force} = \frac{\cos \alpha}{R}. \quad (49)$$

432 The dimensionless ideal-carving equation (34) reads

$$\left(\frac{1}{R^2} - 1\right)^{1/2} = \frac{v^2}{R} - \cos \beta \tan \alpha. \quad (50)$$

433 The equation governing the evolution of β follows from equation (18) upon the sub-
 434 stitution $dl = vdt$. It reads

$$\frac{d\beta}{dt} = \frac{v}{R} \quad (51)$$

435 and the dimensionless skier coordinates can be found via integrating

$$\frac{dx}{dt} = \mp v \cos \beta, \quad (52)$$

436 where we use the sign minus for right turns and the sign plus for left turns, and

$$\frac{dy}{dt} = v \sin \beta. \quad (53)$$

437 Equations (47-53) determine the arc of a carving turn and the skier motion
 438 along the arc. What they do not tell us is when one turn ends and the next one
 439 begins. These transitions have to be introduced independently. In this regard the
 440 angle of traverse is a more suitable independent variable than the time because its
 441 value is a better indicator of how far the turn has progressed. Replacing t with β
 442 via equation (51) we finally obtain the complete system of equations which we use to
 443 simulate carving runs in this study. It includes three ordinary differential equations

$$\frac{dv}{d\beta} = \frac{R}{v} \left(\sin \beta \tan \alpha - \frac{\mu}{R} - Kv^2 \right), \quad (54)$$

444

$$\frac{dx}{d\beta} = \mp R \cos \beta, \quad (55)$$

445

$$\frac{dy}{d\beta} = R \sin \beta, \quad (56)$$

446 and the constitutive equation

$$\left(\frac{1}{R^2} - 1 \right)^{1/2} = \frac{v^2}{R} - \cos \beta \tan \alpha. \quad (57)$$

447 The definition of β implies that it increases both during the left and the right
 448 turns, but not in the transition between turns. In our simplified model of the transi-
 449 tion, the direction of motion \mathbf{u} remains unchanged and hence the angle of traverse has
 450 to change from β to $180^\circ - \beta$. According to equation (57) this implies a jump in the
 451 local turn radius and hence the skier inclination. As a result, during the whole run,
 452 which may consist of many turns, β remains confined between 0° and 180° , provided
 453 each turn terminates before going uphill.

454 Finally, we observe that equations (54) and (57) do not involve x and y and hence
 455 can be solved independently from equations (55-56). However, all these equations
 456 should be integrated simultaneously when we are interested in a skier's trajectory.
 457 Equation (51) should be added as well when we need to know the run evolves in time.

458

Results

459

460

461

462

463

464

465

466

467

Here we present the results of our study of ideal carving runs as described by equations (54-57) with instantaneous transitions between turns. At the start we specify the initial angle of traverse β_{ini} and speed v_{ini} , achieved during the run-up phase. Each turn is terminated when the traverse angle reaches a given value, denoted as β_{fin} . Hence, beginning from the second turn, all turns are initiated at $\beta_{\text{ini}} = 180^\circ - \beta_{\text{fin}}$. Initially we focus on the effect of slope steepness and fix the sidecut parameter to $K = 0.0325$ and the coefficient of friction to $\mu = 0.04$. For the aerodynamic length scale $L_g = 200$ m this corresponds to SL skis with the dimensional radius of $R_{\text{sc}} = 13$ m. Later we discuss the effect of sidecut radius as well.

468

Gentle slope

469

470

471

472

473

474

475

476

477

478

479

480

481

First we consider a slope with $\alpha = 5^\circ$. For such a gentle (“flat”) slope, the speed of fall-line gliding saturates at $v_s = 0.737V_g$. However, the speed limit $V_{\text{sc}} = 0.612V_g < v_s$, indicating that the skier speed may eventually exceed V_{sc} .

Here we present the results for the run with $x_{\text{ini}} = y_{\text{ini}} = 0$, $\beta_{\text{ini}} = 0.3\pi$ (54°), $v_{\text{ini}} = 0.49V_{\text{sc}}$ ($0.3V_g$) and $\beta_{\text{fin}} = 0.9\pi$ (162°). Figure 5 shows the trajectory of this run, which exhibits a rather slow evolution of the turn shape. This agrees with the data presented in Figure 6, which shows the evolution of R , v , Φ and the g-force for the first 20 turns. Indeed, the turn radius does not vary much along the track. Moreover, although each next turn is not an exact copy of the previous turn, for each of the variables we observe convergence to some limiting curve, which will refer to as the asymptotic turn solution. In practical terms, well down the slope each next turn becomes indistinguishable from the previous one. This is reminiscent of the so-called limit cycle solutions in the theory of dynamical systems.

482

483

484

485

486

487

488

Interestingly, the speed of the asymptotic solution remains well below v_s and even below V_{sc} , with the mean value $\langle v \rangle \approx 0.75V_{\text{sc}}$. This is due to the higher work done by the friction force compared to the fall-line gliding because of 1) the longer trajectory of this run compared to the straight fall line and 2) the fact that the effective weight of skier is higher than mg , leading to higher friction force. In order to verify this explanation one can use the equilibrium version of the speed equation (54)

$$\langle \sin \beta \rangle \tan \alpha - \mu \langle \frac{1}{R} \rangle - K \langle v^2 \rangle = 0, \quad (58)$$

where $\langle A \rangle$ stands for the mean turn value of the quantity A . According to figure 6, $\langle 1/R \rangle = \langle \text{g-force} \rangle / \cos \alpha \approx 1.2$ whereas $\langle \sin \beta \rangle$ can be estimated via

$$\langle \sin \beta \rangle = \frac{1}{0.8\pi} \int_{0.1\pi}^{0.9\pi} \sin(\beta) d\beta \approx 0.796.$$

489

Substituting the estimates into equation (58), we find $\langle v \rangle \approx 0.8V_{\text{sc}}$, which is quite

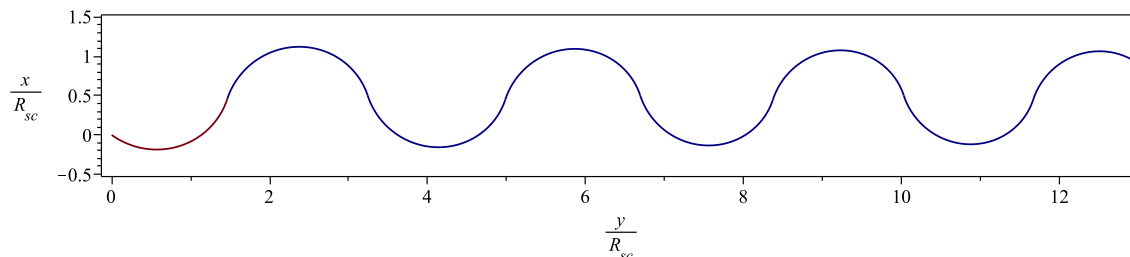


Figure 5. The first few turns of the flat-slope run ($\alpha = 5^\circ$).

490 close to what we see in the numerical data. For $R_{sc} = 13$ m, the corresponding
 491 dimensional value is $\langle v \rangle \approx 27$ km/h.

492 Moderately steep slope

493 Here we deal with a slope with $\alpha = 15^\circ$. For this slope $v_s = 0.922V_g$ and
 494 $V_{sc} = 0.35V_g$ is now significantly below v_s . Figure 7 shows the trajectory of the run
 495 with the same initial parameters and β_{fn} as in the case of flat slope. One can see
 496 that now the turns are much shorter and not so rounded, with the individual turn
 497 shape reminiscent of the letter “J”, rather than “C”. Figure 8 shows the evolution of
 498 R , v , Φ and the g-force for the first 20 turns of this run. Like in the flat-slope case,
 499 the solution converges to an asymptotic one but now this occurs very quickly – the
 500 individual turn curves become indistinguishable beginning from the fourth turn. The
 501 top-left panel of figure 8 confirms that on average the turn radius is significantly lower
 502 than in the flat run. Moreover, it varies dramatically, from $R \approx 0.6R_{sc}$ at the turn
 503 initiation down to $R \approx 0.12R_{sc}$ soon after the fall-line. The latter is approximately
 504 1.6 m (one SL ski length) when the solution is scaled to $R_{sc} = 13$ m.

505 Rather surprisingly, the speed of the asymptotic solution still remains below V_{sc} ,
 506 but only just, and well below V_g . The latter shows that contrary to the expectations
 507 based on the analysis of fall-line gliding, in this slalom run the aerodynamic drag is not
 508 the dominant factor in determining the saturation speed. The reason is the extremely
 509 high effective weight and hence the friction force. According to Figure 8, $\langle 1/R \rangle \approx 5$
 510 and $\langle v \rangle \approx 1$. Hence, in equation (58) the geometric term $\langle \sin \beta \rangle \tan \alpha \approx 0.213$, the
 511 friction term $\langle \mu/R \rangle \approx 0.2$ and the aerodynamic drag term $K\langle v^2 \rangle \approx 0.03$. Thus, the
 512 geometric and the friction terms almost balance each other, whereas the contribution
 513 of the aerodynamic drag is small.

514 The corresponding dimensional value of the mean skier speed in the asymptotic
 515 solution is $v \approx 35$ km/h, which is not that far below the typical speed of slalom
 516 competitions. However, the inclination angle of this run reaches very high values,
 517 $\Phi \approx 80^\circ$ in the lower-c part of the turn and the g-force is extremely high. This shows

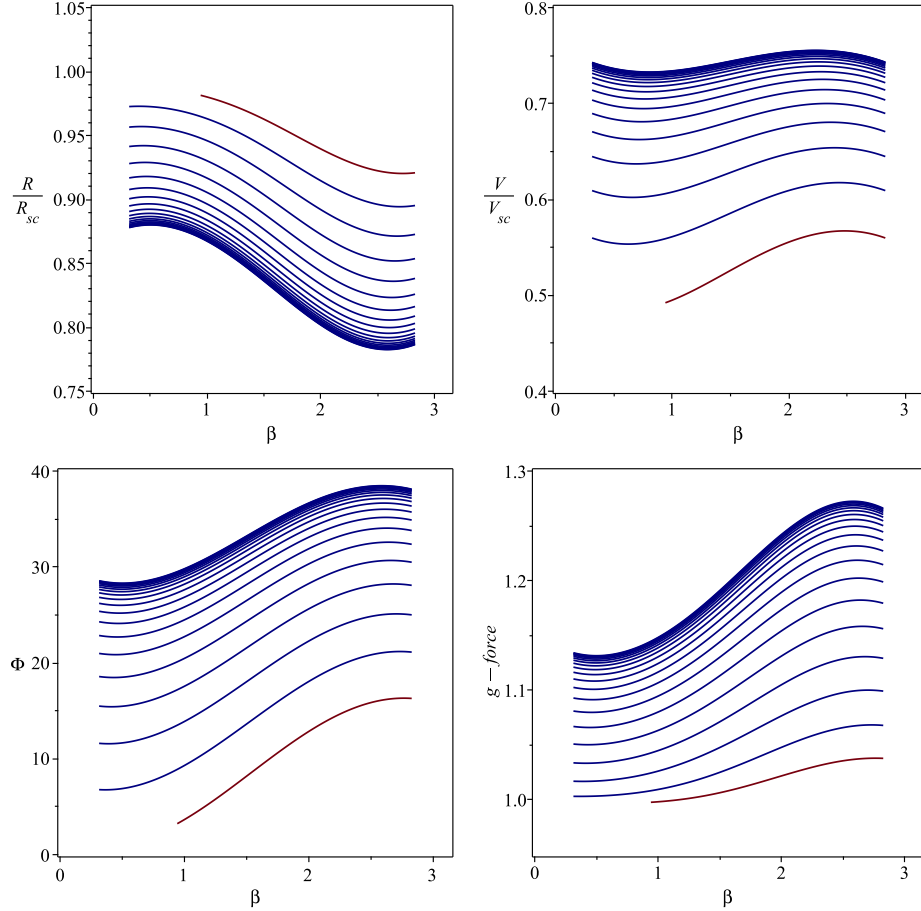


Figure 6. Evolution of $R(\beta)$, $v(\beta)$, $\Phi(\beta)$ and F_n for the flat-slope run ($\alpha = 5^\circ$) during the first 20 turns. In each of these plots, there are 20 curves which show the evolution of these variables during each turn. Each such curve (except the one corresponding to the first turn which originates at $\beta = 0.3\pi$) originates at $\beta = 0.1\pi$ (the turn initiation point) and terminated at $\beta = 0.9\pi$ (the turn completion point). The transition between turns is a jump from the termination point of the previous turn to the initiation point of the next turn. In the R -panel this transition is a jump to the lower curve and in the v -, Φ - and F_n -panels to the upper curve.

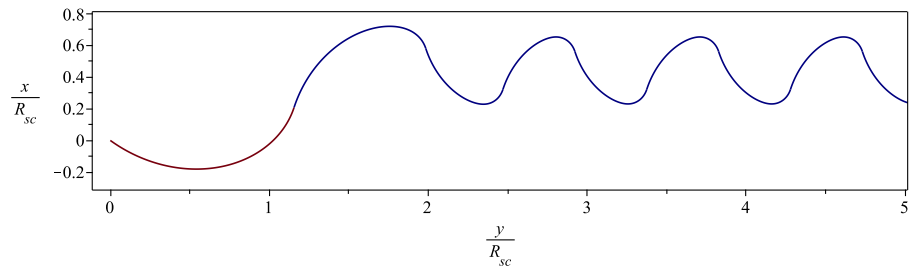


Figure 7. The first few turns for the moderately steep slope ($\alpha = 15^\circ$).

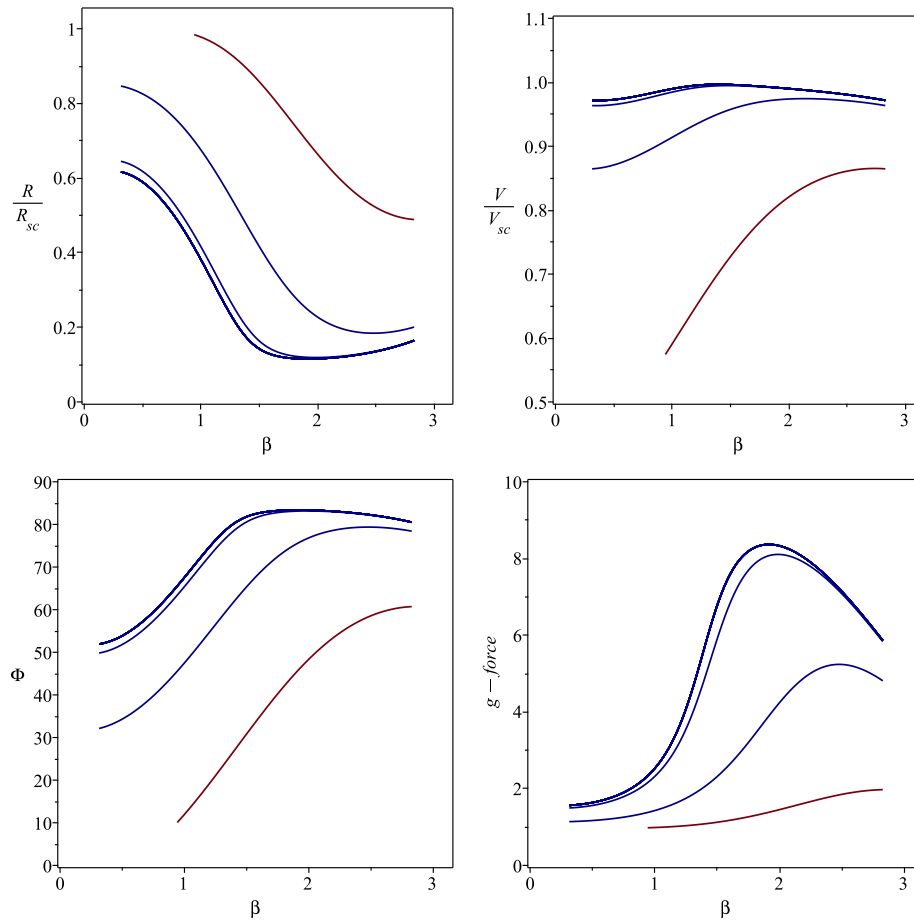


Figure 8. The same as in figure 6 but for the moderately steep slope ($\alpha = 15^\circ$).

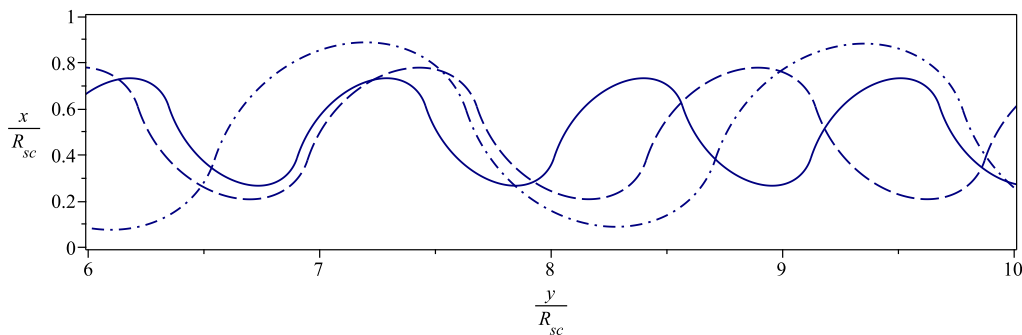


Figure 9. The trajectories of ideal carving runs on the $\alpha = 13^\circ$ slope with slalom (solid), giant slalom (dashed) and downhill (dash-dotted) skis.

518 that in this run we are beyond what is achievable in practice.

519 For a steep slope with $\alpha = 35^\circ$, V_{sc} is reached very quickly and the carving run
 520 cannot be continued beyond the first turn.

521 The approximate similarity of balanced carving runs

522 How different are the carving turns in different alpine disciplines? The equations
 523 of carving turn (54–57) have only three dimensionless parameters that modify these
 524 equations and hence their solutions – the coefficient of dynamic friction μ , the slope
 525 angle α and the dynamic sidecut parameter $K = R_{sc}/L_g \ll 1$. If K was negligibly
 526 small then the equations would be practically non-dependent on R_{sc} . This means
 527 that for the same slope angle and coefficient of friction (the same snow conditions
 528 and wax), the slalom and downhill carving runs would be just scale versions of each
 529 other, with the trajectory scaling as $\propto R_{sc}$, skier’s speed as $\propto V_{sc} \propto \sqrt{R_{sc}}$ and the
 530 g-force and inclination angle both remaining unchanged.

531 Equation (54) tells us that a higher value of K leads to a lower speed in the
 532 asymptotic solution. Because of this and the fact that $K \propto R_{sc}$, we expect v/V_{sc}
 533 to be actually a bit smaller for a discipline where skis have larger R_{sc} . If so then
 534 equation (57) ensures a larger R/R_{sc} , equation (49) a weaker g-force and equation
 535 (33) a smaller inclination angle. To check this, we compared solutions corresponding
 536 to SL, GS (giant slalom) and DH skis for $\alpha = 13^\circ$ and $\mu = 0.04$. Figure 9 shows
 537 the dimensionless trajectories of these runs in the asymptotic regime. Although they
 538 are relatively similar they are still not exact copies of one another, with larger K
 539 yielding longer and smoother turns as expected. Figure 10 shows the behaviour of
 540 other parameters which also agrees with our expectations.

541 In the speed equation (54), K is the coefficient of the aerodynamic drag term
 542 Kv^2 . Hence, the deviation from the simple scaling found in the case $K = 0$ reflects

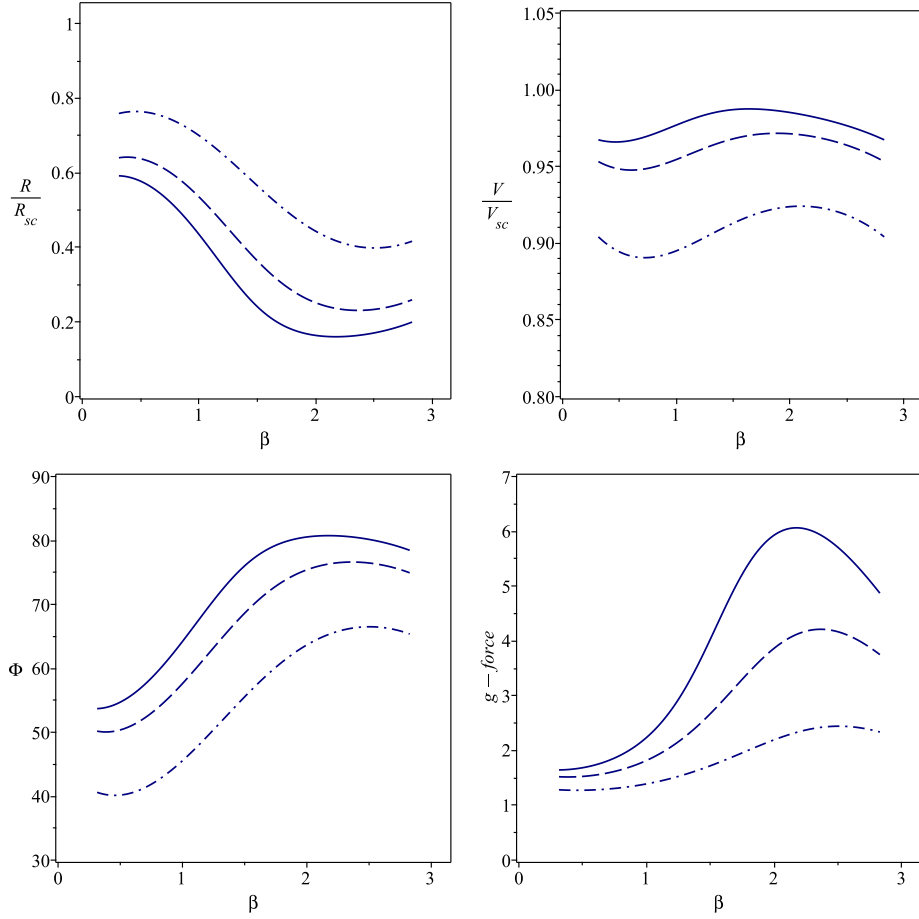


Figure 10. The asymptotic turn parameters for ideal carving runs on the $\alpha = 13^\circ$ slope with slalom (solid), giant slalom (dashed) and downhill (dash-dotted) skis.

543 the variation in the relative importance of the aerodynamic drag. Its role increases
 544 as we move from SL towards DH, which is a well-known fact.

545 **The snow friction and the critical slope gradient**

546 We extended the study described in the previous sections in order to determine
 547 the critical slope steepness $\alpha_{c,t}$ above which pure balanced carving is impossible for
 548 SL, GS and DH skis even theoretically (v exceeds V_{sc}). The result is

$$\alpha_{c,t} = \begin{cases} 17^\circ & \text{for } K = 0.0325 \text{ (13m)}, \\ 19^\circ & \text{for } K = 0.0875 \text{ (30m)}, \\ 21^\circ & \text{for } K = 0.1250 \text{ (50m)}, \end{cases} \quad (59)$$

549 where in the brackets we show the dimensional sidecut radius corresponding to $L_g =$
 550 200m. Here we also observe only a relatively weak dependence on R_{sc} . When the

551 limitations based on the shear resistance of snow, physical strength of skiers and
 552 structural strength of skis are taken into account, the practical critical gradients
 553 become even smaller.

554 The result (59) was obtained for the friction coefficient $\mu = 0.04$. However,
 555 the coefficient depends on many factors and may vary significantly. Since a higher
 556 friction coefficient μ implies a lower saturation speed of the run and hence a weaker
 557 centrifugal force, this may also allow carving on steeper slopes. We explored this
 558 avenue using a little more pragmatic definition of executable carving turns. Namely,
 559 we demanded that the inclination angle Φ did not exceed $\Phi_c = 70^\circ$.

560 We run SL and DH models with $\mu=0.04, 0.07$ and 0.10 . For each model we
 561 used a simple iterative procedure aimed at identifying the slope angle for which in
 562 the asymptotic solution Φ peaked within one percent of Φ_c . The results are shown
 563 in figure 11. They are well fitted by the linear equations

$$\tan \alpha_c = 2.3\mu + 0.06. \quad (60)$$

564 for the SL skis ($K = 0.0325$) and

$$\tan \alpha_c = 2.2\mu + 0.16. \quad (61)$$

565 for the DH skis ($K = 0.125$).

566 The effect of angulation

567 So far we limited our analysis to the case of stacked skier where the skier incli-
 568 nation to the slope (the lever-arm inclination) is the same as the edge angle of their
 569 skis. However, skiers often angulate their body by moving hip and to some degree
 570 knees towards the inside of the turn. In this case, CM shifts from the belly button
 571 towards the outside of the turn and hence the edge angle becomes higher than the
 572 lever-arm inclination (see figure 12). As the torque balance still requires the incli-
 573 nation of the effective gravity force to be the same as the lever arm inclination, this
 574 leads to $\Theta = \Psi - \Phi > 0$.

575 There are at least two benefits of such angulation. Firstly, it is known to
 576 introduce a better safety margin against accidental side-slipping of the skis (skidding).
 577 Secondly, it allows to vary the turn radius, thus introducing some control over the
 578 carving turn (e.g. Harb, 2006; Howe, 1983).

579 We note here that when $\Theta > 0$ the ski is pressed not only against the base of the
 580 platform it creates in the snow but also against the wall of this platform (see figure
 581 12). Hence, the total normal reaction force of the snow $\mathbf{F}_n = \mathbf{F}_{n,b} + \mathbf{F}_{n,w}$ is the sum
 582 of the force $\mathbf{F}_{n,b}$ originated from the base and the force $\mathbf{F}_{n,w}$ originated from the
 583 wall and because of this it may still be aligned with the effective gravity force.

584 Using the notation introduced in our analysis of ICE, $\tan \Psi = (\xi^2 - 1)^{1/2}$ and
 585 $\tan \Phi = a\xi + b$. For $0 < \Phi < \Psi < 90^\circ$, we can write $\tan \Psi = \eta \tan \Phi$ where $\eta > 1$,

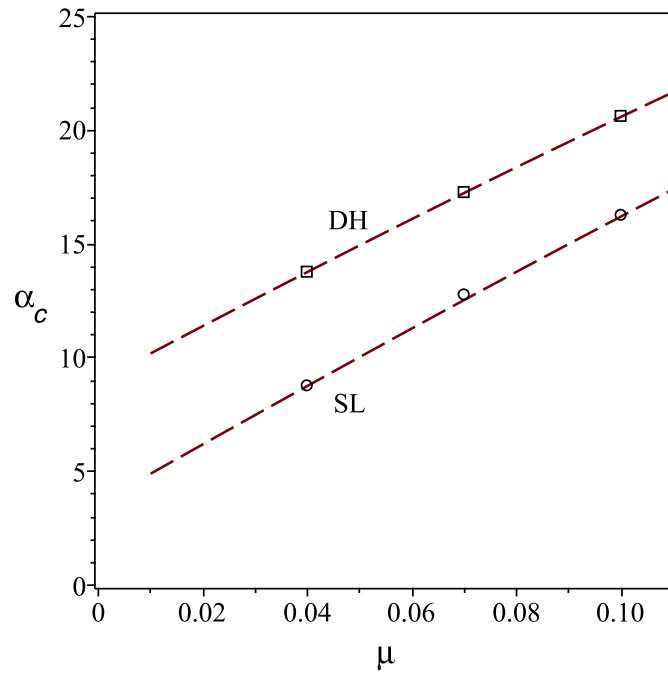


Figure 11. The critical slope gradient as a function of the friction coefficient for $\Phi_c = 70^\circ$. The markers show the numerical data and the dashed lines their fit by the linear functions (60,61).

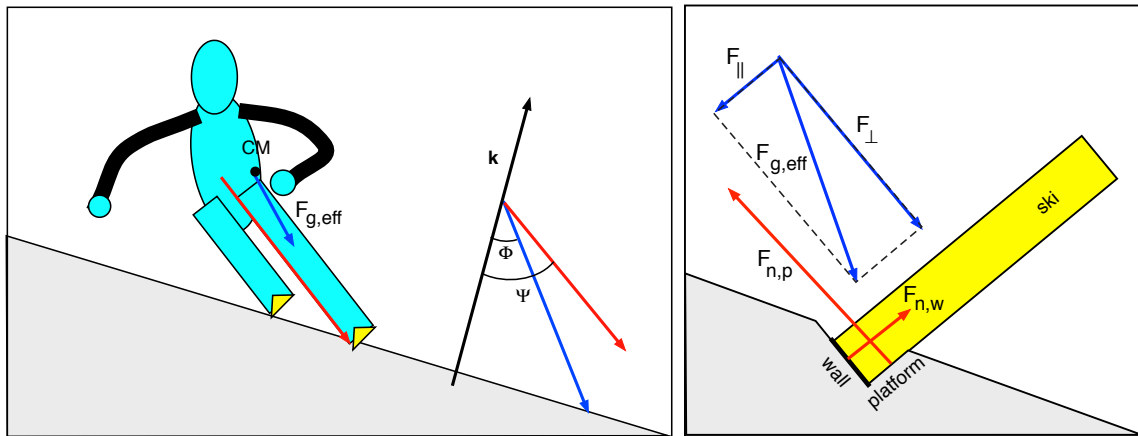


Figure 12. Inclination and angulation. Left panel: Because of the angulation at the hip, the ski edge angle Ψ is higher than the inclination angle of the skier Φ . Right panel: Because $\Psi > \Phi$ the effective gravity has not only the component normal to the platform cut in the snow by the ski (F_{\perp}) but also the component parallel to the platform and pushing the ski into the platform wall (F_{\parallel}). The wall reacts with the force $F_{n,w}$, balancing F_{\parallel} .

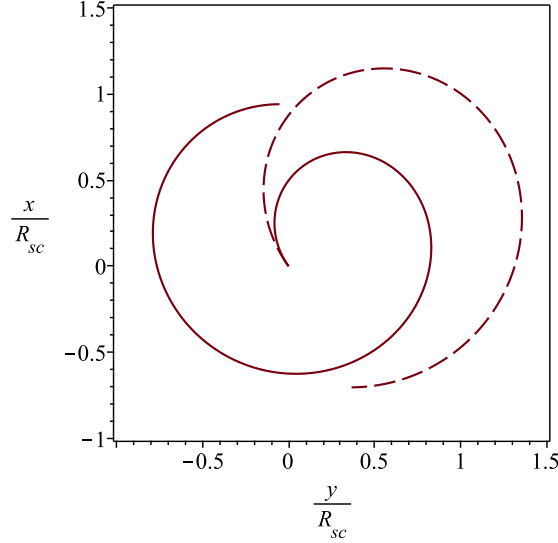


Figure 13. Trajectories of attempted 360° carving turns with (solid line) and without (dashed line) angulation. The trajectory of the turn without angulation terminates at the point where the skier comes to halt, whereas the trajectory of the turn with angulation is terminated arbitrary and the skier speed at the termination point does not vanish.

586 which yields the modified ideal carving equation

$$(\xi^2 - 1)^{1/2} = \eta(a\xi + b). \quad (62)$$

587 Introducing $a' = \eta a > a$ and $b' = \eta b > b$, we can write equation (62) in exactly the
 588 same form as the original ICE (Eq.34) but with the primed parameters in the place
 589 of the original unprimed ones. This immediately allows us to deduce the effect of the
 590 angulation on the speed limits of balanced carving. Since $a + b > 0$ if and only if
 591 $a' + b' > 0$, the lower speed limit (41) remains unchanged. However, the condition
 592 $a' < 1$ now yields the constraint

$$v < V_{sc}(\eta) \quad \text{where} \quad V_{sc}(\eta) = \sqrt{\frac{gR_{sc}}{\eta} \cos \alpha}. \quad (63)$$

593 Thus, the upper speed limit is reduced.

594 In order to elucidate the effect of angulation further, we analysed the so-called
 595 360°-carving turn. By this we understand a carving turn which continues in the
 596 clockwise (or counter-clockwise) direction all the way – first downhill, then uphill and
 597 finally downhill again without any interruption. In this example, we assumed that
 598 the skier angulation depended only on the inclination angle, $\Theta = \Theta(\Phi)$, as described
 599 by the equation

$$\tan \Psi = A + \tan \Phi, \quad (64)$$

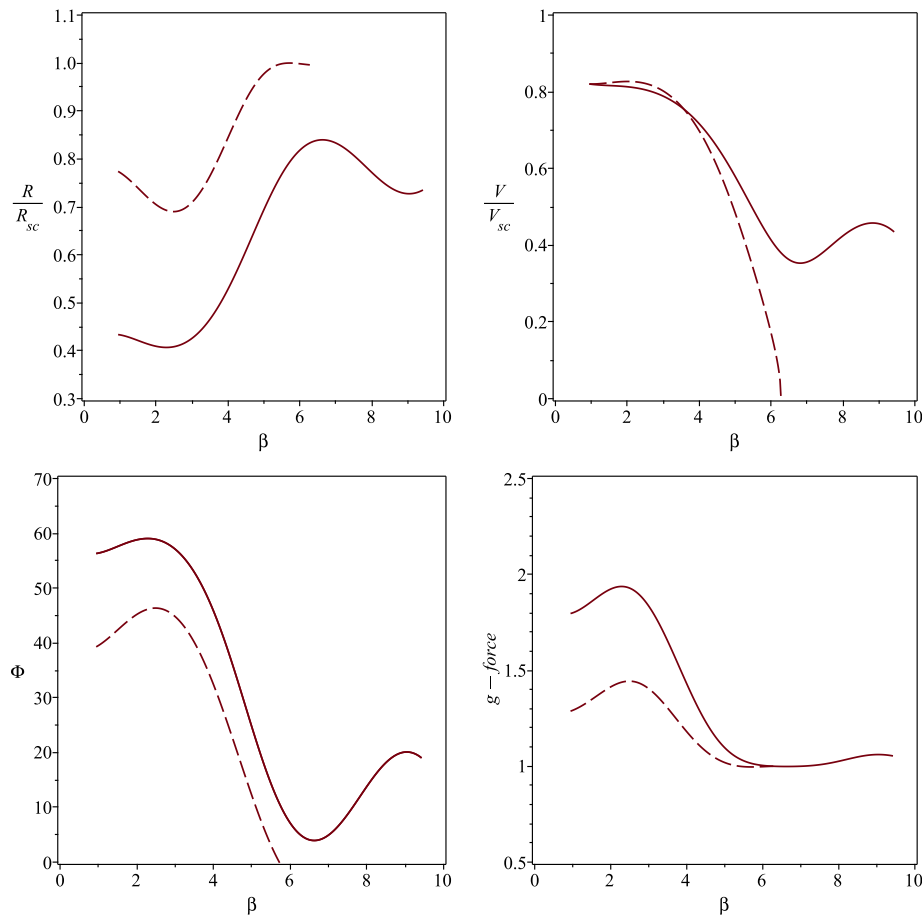


Figure 14. The attempts at 360° turn with (solid lines) and without (dashed lines) angulation.

600 where A is constant. It is easy to see that $A = \tan(\Theta(0))$. It is also easy to verify
 601 that $\Theta(\Phi)$ is a monotonically decreasing function which vanishes as $\Phi \rightarrow 90^\circ$, and
 602 that it yields $\Psi < 90^\circ$ for all $0 \leq \Phi < 90^\circ$.

603 Here we present the results for the slope angle $\alpha = 5^\circ$, the initial skier speed
 604 $v_{ini} = 0.5V_g$ and the initial angle of traverse $\beta_{ini} = 54^\circ$. Such a high speed could
 605 be gained at a preceding steeper uphill section of the slope. Figures 13 and 14 show
 606 the results for two runs: one with no angulation ($A = 0$, dashed lines) and one with
 607 strong angulation ($A = \tan(30^\circ)$, solid lines). The run without angulation falls a bit
 608 short of success. It stops on approach to the summit as the skier's speed drops to
 609 zero. In the run with angulation, the turn is much tighter and the skier reaches the
 610 summit retaining a fair fraction of the initial speed. This allows them to continue
 611 and complete the 360° -turn. Because of the similar initial speed but the lower turn
 612 radius, the centrifugal force, and hence the total g-force of this run, is higher, making
 613 the turn physically more demanding. Moreover, the skier skeleton is no longer well

614 stacked and hence bears a smaller fraction of the total skier's weight. This spells an
615 increased risk of injury.

616 **The effect of loading the inside ski**

617 In our study here, we focused on the case where the skier balances entirely on
618 the inner edge of the ski which is located on the outside of the turn's arc. Indeed, one
619 of the first things learned in ski lessons is keeping most of the load on the outside ski.
620 However, some loading of the inside ski is needed to gain in stability, turn control
621 and reduction of stress on the outside leg.

622 Let us briefly analyse the effect of partial loading of the inside ski in carving
623 turns. Denote as $\mathbf{F}_{n,i}$ and $\mathbf{F}_{n,o}$ the normal reaction forces from the inside and the
624 outside skis, respectively, and as \mathbf{r}_i and \mathbf{r}_o the position vectors connecting the skier's
625 CM with the inner edges of the skis in the transverse plane. The force balance then
626 reads

$$\mathbf{F}_{g,\text{eff}} + \mathbf{F}_{n,i} + \mathbf{F}_{n,o} = 0, \quad (65)$$

627 whereas the torque balance in the transverse plane is

$$\mathbf{r}_i \times \mathbf{F}_{n,i} + \mathbf{r}_o \times \mathbf{F}_{n,o} = 0. \quad (66)$$

Provided the shanks of both legs are parallel to each other, equation (65) implies

$$\mathbf{F}_{n,i} = -a\mathbf{F}_{g,\text{eff}} \quad \text{and} \quad \mathbf{F}_{n,o} = (a-1)\mathbf{F}_{g,\text{eff}},$$

where $0 \leq a \leq 1$. Substituting these into equation (66), we obtain

$$\mathbf{F}_{g,\text{eff}} \times (a\mathbf{r}_i + (1-a)\mathbf{r}_o) = 0$$

and hence

$$\mathbf{F}_{g,\text{eff}} = A(\mathbf{r}_o + a(\mathbf{r}_i - \mathbf{r}_o)).$$

628 Thus in balanced stance, $\mathbf{F}_{g,\text{eff}}$ points to the inner edge of the outside ski when $a = 0$,
629 to the inner edge of the inside ski when $a = 1$ and to somewhere in between when
630 $0 < a < 1$. Since $a > 0$ implies $\Phi < \Psi$, the effect of loading of the inside ski is
631 similar to the effect of the angulation. In particular, the upper speed limit is reduced
632 compared to the case where only the outside ski is loaded. In order to ski in balance
633 at speeds exceeding this reduced speed limit, the loading of the inside ski should
634 decrease, $a \rightarrow 0$.

635 **Discussion and Implications**

636 In this paper we described a simple mathematical model of balanced carving
637 turns in alpine skiing, which can be applied to snowboarding as well. The model
638 combines a system of ordinary differential equations governing the CM motion with
639 the so-called Ideal Carving Equation (ICE), which emerges from the analysis of the

640 skier balance in the frontal plane. ICE relates the local radius of the CM trajectory
 641 to skier's speed and direction of motion relative to the fall line and hence provides
 642 closure to the system.

643 In the case of fall-line gliding, the skier speed grows until the gravity force is
 644 balanced by the aerodynamic drag and snow friction forces. Unless the slope is of
 645 very low gradient, the snow friction is a minor factor and can be ignored, whereas the
 646 balance between the gravity and the aerodynamic drag yields the saturation speed
 647 V_g . For this reason, V_g and the distance L_g required to reach it could be considered
 648 as the characteristic scales of alpine skiing. However, in the case of balanced carving
 649 turns, ICE introduces another characteristic speed, the carving speed limit V_{sc} . When
 650 the skier speed exceeds V_{sc} , the balance of forces acting on the skier can no longer
 651 be sustained. Because as a rule V_{sc} is lower than V_g , this suggests that V_{sc} is more
 652 relevant in the dynamics of carving turns. Moreover, the radius of carving turns
 653 cannot exceed the ski sidecut radius R_{sc} , making the latter a natural length scale of
 654 this dynamics. These two scales lead to the dimensionless equations of carving turn
 655 which have only three dimensionless control parameters: the slope gradient angle α ,
 656 the dynamic coefficient of friction μ and the dynamic sidecut parameter $K = R_{sc}/L_g$,
 657 which appears as a coefficient of the term, Kv^2 , describing the aerodynamic drag
 658 force.

659 We used the model to explore ski runs composed of linked carving turns on a
 660 slope with constant gradient. While in reality such turns are linked via a transition
 661 phase of finite duration, in our simulations the transitions are instantaneous and take
 662 place at a specified traverse angle (the angle between the skier trajectory and the fall
 663 line). At the transition, the skier speed and direction of motion remain invariant,
 664 whereas the inclination angle and hence the turn radius jump to the values corre-
 665 sponding to the next turn. Under these conditions, the solution either approaches a
 666 limit cycle, where the turns become indistinguishable one from another, or terminates
 667 after reaching the speed limit V_{sc} .

668 When measured in the units of R_{sc} and V_{sc} , the balanced carving solutions
 669 corresponding to $13\text{m} < R_{sc} < 50\text{m}$ are rather similar. This is because 1) R_{sc}
 670 enters the problem only via the dynamic sidecut parameter $K = R_{sc}/L_g \ll 1$ which
 671 determines the relative strength of the aerodynamic drag force, and 2) for $V < V_{sc}$
 672 this force remains relatively small. Yet the drag term is not entirely negligible and
 673 the solutions show some mild variation with R_{sc} . In particular, turns corresponding
 674 to a larger sidecut radius are less extreme, with smaller inclination angles and weaker
 675 g-forces.

676 Our results show the existence of a critical slope angle $\alpha_{c,t}$ above which the
 677 speed of balanced ideal carving run eventually exceeds V_{sc} . The value of $\alpha_{c,t}$ depends
 678 on the coefficient of friction μ and to a lesser degree on the sidecut parameter of the
 679 skis. For $\mu = 0.04$ we find $\alpha_{c,t} = 17^\circ$ for SL skis, 19° for GS skis and 21° for DH skis.
 680 In practice, a number of factors, such as the hardness of snow, structural integrity of
 681 skis and strength of human body, come into play well before this theoretical limit and

682 restrict balanced carving to slopes of even lower gradient. For example, demanding
 683 that the skier inclination angle remains below $\Phi_c = 70^\circ$ (and hence the g-force below
 684 three), we find that for SL skis the critical inclination angle $\alpha_c \approx 9^\circ$ if $\mu = 0.04$ and
 685 $\alpha_c \approx 16^\circ$ if $\mu = 0.1$. For DH skis the corresponding values are $\alpha_c \approx 14^\circ$ and 21° .
 686 Overall, we find that the critical gradient increases linearly with μ .

687 Slopes of sub-critical gradient can be roughly divided into the gentle and moder-
 688 ately steep groups. For slopes of gentle gradient (aka “flat slopes”), the aerodynamic
 689 drag is not dominant over the snow friction even in the case of fall-line gliding and in
 690 carving runs the turn speed saturates well below both V_g and V_{sc} . The carved arcs
 691 are nearly circular and their radius is only slightly below the sidecut radius of the
 692 skis. The skier inclination angle and the g-force stay relatively small.

693 On slopes of moderate gradient the saturation speed of fall-line gliding is close
 694 to V_g , which is significantly above V_{sc} . However, the speed of carving runs saturates
 695 near V_{sc} , mostly because of the frictional energy losses. The closeness to the speed
 696 limit makes the carving turns quite extreme. Their shape deviates from the rounded
 697 shape of the letter C and reminds the letter J instead, with the local turn curvature
 698 significantly increasing on the approach to the fall line. As the curvature increases,
 699 the centrifugal force and hence the total g-force experienced by the skier grow. In
 700 order to stay in balance, they have to adopt large inclination to the slope. The
 701 significantly increased effective gravity leads to high normal reaction from the snow
 702 and hence significantly increased friction, which is the reason why the speed stays
 703 well below V_g .

704 On slopes of super-critical gradient ($\alpha > \alpha_c$) the speed quickly exceeds V_{sc} ,
 705 after which the balanced carving cannot be continued.

706 The fact that balanced carving requires ski slopes to be rather gentle (of the
 707 green gradient in the US colour-coding scheme) is interesting as most slopes of ski
 708 resorts are steeper, not to mention typical race tracks. In conflict with this, skillful
 709 skiers manage to execute on such slopes at least partly carved turns. One possible
 710 explanation is that they use the skidding phase of their hybrid turns to slow down
 711 and keep their speed below V_{sc} . This may be true for recreational skiers but not so
 712 for top racers in competitive runs. In Table 1 we show average speeds achieved in
 713 FIS World Cup races (Gilgien, Crivelli, Spörri, Kröll, & Müller, 2015; Gilgien et al.,
 714 2014; Supej et al., 2014) as well as the speed limit V_{sc} calculated using equation
 715 (40), which can be written in the following convenient form:

$$V_{sc} = 40 \left(\frac{R_{sc}}{13 \text{ m}} \right)^{1/2} \left(\frac{\cos \alpha}{\cos 15^\circ} \right)^{1/2} \text{ km h}^{-1}. \quad (67)$$

716 One can see that in all the disciplines, the average racer speed exceeds the upper
 717 speed limit of balanced carving. Obviously, on fast sections of race course the conflict
 718 is even stronger. For example, in downhill competitions the current speed record is
 719 $v = 162 \text{ km h}^{-1}$ (racer Johan Clarey, Wengen track). This comparison shows that the
 720 restrictions set by the theory of balanced pure carving are not consistent with the

Table 1

Parameters of race runs (Gilgien et al., 2015, 2014; Supej et al., 2014). R_{sc} is the sidecut radius of skis, α is the inclination angle of the slope, $\langle L_v \rangle$ and $\langle L_h \rangle$ are the mean separations between the gates down the fall line and across the fall line, respectively, R_a is the radius of the arc defined by the mean gate separations, V is the skier speed, $\zeta = \langle V \rangle^2 / g R_{sc}$ is a dimensionless speed parameter and L_g is the distance along the fall line required to reach the speed $\langle V \rangle$.

Parameter	SL	GS	SG	DH
$\langle \alpha \rangle$ [°]	20	18 ± 7	17 ± 7	14 ± 8
R_{sc} [m]	≤ 15	27	33	45
R_{min} [m]	7	8.4	17.2	20.6
$\langle V \rangle$ [km/h]	45	62	82	86
V_{sc} [km/h]	43	57	63	75

721 practice of alpine ski racing and some of the assumptions made in the theory are not
722 quite valid and require critical examination.

723 One of the most obvious weaknesses of the model is that it cannot describe
724 self-consistently the transition phase between carving turns. Such a transition does
725 not arise naturally as a part of the solution of differential equations. Instead, it is
726 introduced somewhat arbitrary as a link between two different solutions describing two
727 different arcs of balanced carving. If the solution describing an arc is not terminated,
728 the arc will continue uphill until the skier stops. The reason for this is that in the
729 transition a skier cannot not be in balance and hence one has to go beyond the
730 assumption of balanced carving in order to deal with it.

731 Even the modelling of a single turn is not entirely self-consistent. On the one
732 hand, the model assumes that at every point of the turn the total torque acting on the
733 skier vanishes. On the other hand, the balance condition yields the skier inclination
734 that varies throughout the turn, which can only be the case if the torque does not
735 vanish. This shows that in reality the balance can be only approximate. The model
736 may still be relevant provided the characteristic time of reaching balance is much
737 shorter than the turn duration but in order to verify this condition a more advanced
738 theory is required.

739 Our analysis of the case with $v > V_{sc}$ shows that for such high speeds the
740 net torque pushes skier upwards, towards the position perpendicular to the slope, no
741 matter what the skier inclination to the slope is. In other words, the centrifugal force
742 always dominates gravity. This suggests that in this regime the dynamics of skier's
743 body may be similar to that of a pendulum, with its natural oscillations about the
744 vertical position.

745 Another obvious fact is that the typical speed of even elite racers is much lower
746 than the limit set by the drop of potential energy and air resistance. As the wet snow
747 friction is very low, this implies another channel of energy dissipation which is not

748 included in our model but plays a key role in the dynamics of a typical ski turn. As
749 we have stated in the introduction, the typical turn is hybrid in nature and involves
750 a significant degree of skidding in its initial phase. The high effective coefficient of
751 friction associated with skidding (Sahashi & Ichino, 1998) shows that the skidding
752 phase is most likely to be responsible for most of the energy dissipation in hybrid
753 turns.

754 Conclusion

755 In this paper we explored in detail the model of carving turns in alpine skiing
756 and snowboarding based on the usual assumption of approximate balance between
757 forces and torques acting on the skier during the turn. In its basic form the model was
758 proposed by Jentschura and Fahrbach (2004), where it was implicitly assumed that
759 the skier was stacked and only one of the skis was loaded. We confirm the conclusion
760 of Jentschura and Fahrbach (2004) that the approximation of torque balance yields
761 an upper limit on the skier speed and show that it imposes a lower limit as well,
762 with both these limits depending only on the sidecut radius of skis and the slope
763 gradient. We use the model to simulate carving runs on slopes of constant gradient
764 and find that in this model carving is possible only on relatively flat slopes, with the
765 critical slope angle in the range of $8^\circ - 20^\circ$. The exact value depends mostly on the
766 coefficient of snow friction and to a lesser degree on the sidecut radius of skis. We
767 have extended the analysis to the case of an angulated skier and the case where both
768 skis are loaded and found that in these cases the upper limits on the skier speed and
769 the slope gradient are even more restrictive. This is in conflict with the practice of ski
770 racing which demonstrates that carving is possible at higher speeds and on steeper
771 slopes than the model allows. Our analysis of the torques exerted by the gravity and
772 centrifugal forces shows that when the skier speed exceeds the upper limit of balanced
773 carving, the lifting torque due to centrifugal force wins over the lowering torque of the
774 gravity for any inclination angle of the skier. This suggests the possibility of carving
775 runs where skiers swing from one side to another without settling to an equilibrium at
776 any point of the turn, like a pendulum. A more advanced theory is needed to assess
777 this hypothesis.

778 Acknowledgments

779 The non-trivial calculations of this study were carried out with the software
780 package *Maple* (Maple is a trademark of Waterloo Maple Inc.).

Appendix A

Edge radius of flexed skis

781 Here we analyse the geometry of a carving ski and how it changes when placed at the
782 edge angle Ψ to a flat surface, which we assume to be hard and hence not changed
783 in the process apart from a small cut possibly made in it by the ski's sharp steel

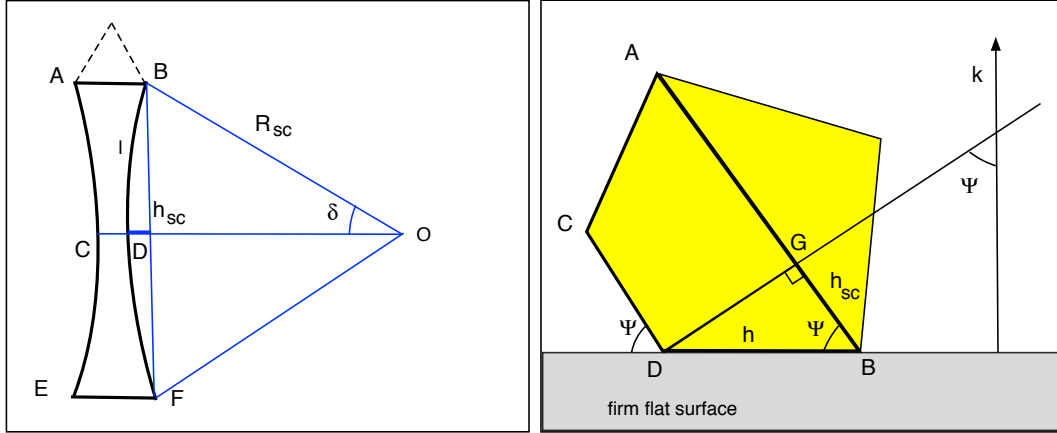


Figure A1. *Left panel:* Shaped ski, its sidecut h_{sc} and sidecut radius R_{sc} . The dashed line shows the ski tip which is not important for determining R_{sc} . *Right panel:* The same ski with the edge BDF pressed against a hard flat surface at the edge angle Ψ as seen in projection on the plane normal to the ski at its waist. In this projection, DGB is a right-angle triangle.

784 edges. We start with the case where the ski lays flat as shown in the left panel of
 785 figure A1. In the figure, the ski is highly symmetric with no difference between its
 786 nose and tail sections. Although the real skis are wider at the nose this does not
 787 matter as long as their running edges can be approximated as circular arcs of radius
 788 R_{sc} , called the sidecut radius. Denote as D the point in the middle of the edge BF
 789 and as l the distance between B and D (or A and C) along the edge. As seen in
 790 this figure, $l = R_{sc}\delta$, where δ is the angular size of the edge DB as seen from its
 791 centre of curvature. This angle is normally rather small. For an SL ski of length
 792 $l_{ski} \approx 2l = 1.65$ m and $R_{sc} = 12.7$ m we have $\delta \approx 0.065$ (3.7°). For other kinds of
 793 racing skis, it is even smaller. The sidecut depth h_{sc} is defined as the distance between
 794 D and the straight line BF connecting the opposite ends of the edge. Obviously,

$$h_{sc} = R_{sc}(1 - \cos \delta). \quad (68)$$

Using the first two terms of the Maclaurin expansion for $\cos \delta$

$$\cos \delta = 1 - \frac{1}{2}\delta^2 + O(\delta^4)$$

795 and then substituting $\delta = l/R_{sc}$ one finds the approximation

$$h_{sc} \simeq \frac{l^2}{2R_{sc}}. \quad (69)$$

796 Now suppose that this ski is kept at the angle Ψ to a firm flat surface and
 797 that it is pressed in the middle until its lower edge comes into the contact with the

798 surface along its whole length (excluding the tip). In this position the edge can still be
 799 approximated as an arc but a different one. Denote its radius as R_e and its “sidecut”
 800 depth as h (see the right panel of figure A1). Obviously R_e and h are connected in
 801 the same way as R_{sc} and h_{sc}

$$h = R_e(1 - \cos \delta) . \quad (70)$$

802 where now $\delta = l/R_e$. When $\delta \ll 1$, this is approximated as

$$h \simeq \frac{l^2}{2R_e} \quad (71)$$

803 and hence

$$\frac{R_e}{R_{sc}} = \frac{h_{sc}}{h} . \quad (72)$$

804 Analysing the right angle triangle GDB of the right panel in figure A1, one finds that
 805 $h_{sc} = h \cos \Psi$ and hence

$$\frac{R_e}{R_{sc}} = \cos \Psi . \quad (73)$$

806 This is the same as equation (9-4) in Howe (1983) and equation (3.7) in Lind and
 807 Sanders (1996).

Appendix B

Lateral stability

808 Here we analyse the stability of skier’s balanced position in the transverse plane,
 809 focusing on the simplified case of loading only the outside ski.

810 We first consider the stability of a stacked skier. Suppose that in the equilibrium
 811 position the ski edge angle and the inclinations angle of the skier are Ψ_0 and $\Phi_0 = \Psi_0$
 812 respectively. Hence,

$$\tan \Psi_0 = (\xi_0^2 - 1)^{1/2} , \quad \tan \Phi_0 = a\xi_0 + b , \quad (74)$$

813 where ξ_0 stands for the equilibrium turn radius. Consider a perturbation that changes
 814 the ski angulation position but keeps the skier velocity unchanged (and hence a and
 815 b as well). However, the turn radius changes and so does the effective gravity. We
 816 need to determine if the modified effective gravity is a restoring force or ti pushes
 817 the system further away from the equilibrium. In the perturbed state $\Psi = \Psi_0 + \delta\Psi$,
 818 $\Psi = \Phi_0 + \delta\Phi$ and $\xi = \xi_0 + \delta\xi$, where δA stands for the perturbation of A . It is clear
 819 that when $\delta\Psi > 0$ the instability condition reads $\Psi > \Phi$ or $\delta\Psi > \delta\Phi$, whereas for
 820 $\delta\Psi > 0$ it is $\delta\Psi < \delta\Phi$. Both these cases are captured in the instability condition

$$\frac{\delta\Phi}{\delta\Psi} < 1 . \quad (75)$$

821 Using equation (74) we find

$$\delta(\tan \Psi) = \frac{\xi_0}{\tan \Psi_0} \delta\xi, \quad (76)$$

822 and

$$\delta(\tan \Phi) = a\delta\xi. \quad (77)$$

823 Hence,

$$\frac{\tan \delta\Phi}{\tan \delta\Psi} = \frac{a \tan \Psi_0}{\xi_0} = a \sin \Psi_0. \quad (78)$$

824 According to the condition (40), in carving turns $a < 1$ and hence equation (78)
825 immediately yields $\tan \delta\Phi / \tan \delta\Psi < 1$. This implies $\delta\Phi / \delta\Psi < 1$ and therefore we
826 conclude the lateral equilibrium is unstable.

827 While the balance of an angulated skier is still unstable, in this case there is
828 an additional way of controlling the instability, namely by a suitable change of the
829 angulation. If $\delta\Psi$ is the perturbation of the ski edge angle and $\delta\Phi$ is the corresponding
830 perturbation of the effective gravity angle that the skier can restore their balance via
831 changing their angulation by the amount

$$\delta\psi = \delta\Psi - \delta\Phi. \quad (79)$$

832

References

- 833 Brown, C. (2009). Modeling edge-snow interactions using machining theory. In E. Müller,
834 L. S., & T. Stöggl (Eds.), *Science and skiing iv* (p. 175-182). Maidenhead, UK: Meyer
835 & Meyer Sport.
- 836 Colbeck, S. (1992). *A review of the processes that control snow friction* (Tech. Rep.).
837 Hanover, NH: Cold Regions Research and Engineering Laboratory (CRREL). Re-
838 trieved from <https://apps.dtic.mil/sti/citations/ADA252362>
- 839 Federolf, M., Lüthi, P., Roos, A., & Dual, J. (2010). Parameter study using a finite element
840 simulation of a carving alpine ski to investigate the turn radius and its dependence
841 on edging angle, load, and snow properties. *Sports Eng.*, *12*, 135-141.
- 842 Federolf, P., Roos, M., Lüthi, A., & Dual, J. (2010). Finite element simulation of the ski-
843 snow interaction of an alpine ski in a carved turn. *Sports Engineering*, *12*, 123-133.
- 844 Gilgien, M., Crivelli, P., Spörri, J., Kröll, J., & Müller, E. (2015). Characterization of
845 course and terrain and their effect on skier speed in world cup alpine ski racing. *PLoS*
846 *ONE*, *10*, e0118119.
- 847 Gilgien, M., Spörri, J., Kröll, J., Crivelli, P., & Müller, E. (2014). Mechanics of turning
848 and jumping and skier speed are associated with injury risk in men's world cup alpine
849 skiing: a comparison between the competition disciplines. *British Journal of Sports*
850 *Medicine*, *48*, 742-747.
- 851 Harb, H. (2006). *Essentials of skiing*. New York: Hatherleigh Press.
- 852 Hirano, Y. (2006). Quickest descent line during alpine ski racing. *Sports Eng.*, *9*, 221.
- 853 Howe, J. (1983). *Skiing mechanics*. Laporte, Colorado: Poudre Press.

- 854 Jentschura, U., & Fahrbach, F. (2004). Physics of skiing: The ideal carving equation and
855 its applications. *Canadian Journal of Physics*, *82*, 249.
- 856 Landau, L., & Lifshitz, E. (1969). *Mechanics*. Oxford: Pergamon Press.
- 857 LeMaster, R. (2010). *Ultimate skiing*. Champaign: Human Kinetics.
- 858 Lind, D., & Sanders, S. (1996). *The physics of skiing: Skiing at the triple point*. New York:
859 Springer-Verlag.
- 860 Merchant, M. (1945). Mechanics of the metal cutting process. i. orthogonal cutting and a
861 type 2 chip. *J. Appl. Phys.*, *16*, 267-275.
- 862 Mössner, M., Heinrich, D., Kaps, P., Schretter, H., & Nachbauer, W. (2008). Computer
863 simulation of consecutive ski turns. *Journal of ASTM International*, *5*(8), 1.
- 864 Mössner, M., Heinrich, D., Kaps, P., Schretter, H., & Nachbauer, W. (2009). Effects of ski
865 stiffness in a sequence of ski turns. In E. Müller, L. S., & S. T. (Eds.), *Science and*
866 *skiing iv* (p. 374). Waterford, Maine: McIntire Publishing.
- 867 Mössner, M., Heinrich, D., Schindelwig, K., Kaps, P., Lugner, P., Schmiedmayer, H.-B.,
868 ... Nachbauer, W. (2006). Modeling of the ski-snow contact for a carved turn. In
869 E. Moritz & S. Haake (Eds.), *Engineering of sport 6* (p. 195). New York: Springer.
- 870 Mössner, M., Innerhofer, G., Schindelwig, K., Kaps, P., Schretter, H., & Nachbauer, W.
871 (2013). Measurement of mechanical properties of snow for simulation of skiing.
872 *J. Glaciology*, *59*, 1170-1178.
- 873 Nachbauer, W., Kaps, P., Hasler, M., & Mössner, M. (2016). Friction between ski and snow.
874 In F. Braghin, C. F., S. Maldifassi, & S. Melzi (Eds.), *The engineering approach to*
875 *winter sports* (p. 33). New York: Springer.
- 876 Nordt, A., Springer, G., & Kollár, L. (1999). Simulation of a turn on alpine skis. *Sports*
877 *Engineering*, *2*, 181-199.
- 878 Oberegger, U., Kaps, P., Mössner, M., Heinrich, D., & Nachbauer, W. (2010). Simulation
879 of turns with a 3d skier model. *Procedia Engineering*, *2*(2), 3171-3177.
- 880 Reid, R. (2010). *A kinematic and kinetic study of alpine skiing technique in*
881 *slalom*. PhD dissertation, Norwegian School of Sport Sciences. Retrieved from
882 <http://hdl.handle.net/11250/171325>
- 883 Reid, R. C., Haugen, P., Gilgien, M., Kipp, R. W., & Smith, G. A. (2020). Alpine ski motion
884 characteristics in slalom. *Frontiers in Sports and Active Living*, *2*, 25. Retrieved
885 from <https://www.frontiersin.org/article/10.3389/fspor.2020.00025> doi:
886 10.3389/fspor.2020.00025
- 887 Rudakov, R., Lisovski, A., Ilyalov, O., & Podgaets, R. (2010). Optimisation of the skier's
888 trajectory in special slalom. *Procedia Engineering*, *2*, 3179-3182.
- 889 Sahashi, T., & Ichino, S. (1998). Coefficient of kinetic friction of snow skis during turning
890 descents. *Japanese Journal of Applied Physics*, *37*, 720-727.
- 891 Spörri, J., Kröll, J., Gildien, M., & Müller, E. (2016). Sidecut radius and the mechanics of
892 turning equipment designed to reduce risk of severe traumatic knee injuries in alpine
893 giant slalom ski racing. *Br. J. Sports Med.*, *50*, 14-19.
- 894 Supej, M., Hebert-Losier, K., & Holmberg, H.-C. (2014). Impact of the steepness of the
895 slope on the biomechanics of world cup slalom skiers. *International Journal of Sports*
896 *Physiology and Performance*, *10*, 361-368.
- 897 Tada, N., & Hirano, Y. (2002). In search of the mechanics of a turning alpine ski using
898 snow cutting force measurements. *Sports Engineering*, *5*, 15-22.

- 899 Yoneyama, T., Scott, N., Kagawa, H., & Osada, K. (2008). Ski deflection measurement
900 during skiing and estimation of ski direction and edge angle. *Sports Engineering, 11*,
901 3-13.